



New insight into the formation and aging processes of organic aerosol from positive matrix factorization (PMF) analysis of ambient FIGAERO-CIMS thermograms

Mingfu Cai^{1,2,3}, Bin Yuan^{2,3}, Weiwei Hu^{4,5}, Ye Chenshuo⁶, Shan Huang^{2,3}, Suxia Yang⁷, Wei Chen⁴, Yuwen Peng^{2,3}, Zhaoxiong Deng^{2,3}, Jun Zhao^{8,✉}, Duohong Chen⁹, Jiaren Sun¹, and Min Shao^{2,3}

¹Guangdong Province Engineering Laboratory for Air Pollution Control, Guangdong Provincial Key Laboratory of Water and Air Pollution Control, South China Institute of Environmental Sciences, MEE, Guangzhou 510655, China

²Institute for Environmental and Climate Research, Jinan University, Guangzhou 511443, China

³Guangdong-Hongkong-Macau Joint Laboratory of Collaborative Innovation for Environmental Quality, Jinan University, Guangzhou 510632, China

⁴State Key Laboratory of Advanced Environmental Technology, Guangzhou Institute of Geochemistry, Chinese Academy of Sciences, Guangzhou 510640, China

⁵Guangdong-Hong Kong-Macao Joint Laboratory for Environmental Pollution and Control, Guangzhou Institute of Geochemistry, Chinese Academy of Science, Guangzhou 510640, China

⁶Guangdong Provincial Academy of Environmental Science, Guangzhou 510045, China

⁷Guangzhou Research Institute of Environment Protection Co., Ltd, Guangzhou 510620, China

⁸School of Atmospheric Sciences, Guangdong Province Key Laboratory for Climate Change and Natural Disaster Studies, and Institute of Earth Climate and Environment System, Sun Yat-sen University, Zhuhai 519082, China

⁹Guangdong Environmental Monitoring Center, Guangzhou 510308, China

✉deceased, October 2024

Correspondence: Weiwei Hu (weiwei@gsig.ac.cn)

Received: 18 September 2025 – Discussion started: 5 October 2025

Revised: 29 December 2025 – Accepted: 5 January 2026 – Published: 15 January 2026

Abstract. Secondary organic aerosol (SOA) is an important component of organic aerosol (OA), yet its atmospheric evolution and impacts on volatility remain poorly understood. In this study, we investigated the volatility of different types of SOA at a downwind site of the Pearl River Delta (PRD) region in the fall of 2019, using a time-of-flight chemical ionization mass spectrometer coupled with a Filter Inlet for Gases and Aerosol (FIGAERO-CIMS). Positive matrix factorization (PMF) analysis was performed on the thermogram data of organic compounds (referred as FIGAERO-OA) measured by the FIGAERO-CIMS. Eight factors were resolved, including six daytime chemistry related factors, a biomass burning related factor (BB-LVOA, 10 % of the FIGAERO-OA), and a nighttime chemistry related factor (Night-LVOA, 15 %) along with their corresponding volatility. Day-HNO_x-LVOA (12 %) and Day-LNO_x-LVOA (11 %) were mainly formed through gas-particle partitioning. Increasing NO_x levels mainly affected SOA formation through gas-particle partitioning, suppressing the formation of low-volatile organic vapors, and thus promoting the formation of relatively high volatile OA with a higher N : C ratio. Two aged OA factors, Day-aged-LVOA (16 %) and Day-aged-ELVOA (11 %), were attributed to daytime photochemical aging of pre-existing OA. In addition, the daytime formation of Day-urban-LVOA (16 %) and Day-urban-ELVOA (7 %) could only be observed in the urban plume. Results show that both gas-particle partitioning (36 %) and photochemical aging (30 %) accounted for a major fraction in FIGAERO-OA in the afternoon during the urban air masses period, especially for high-NO_x-like pathway (~21 %). In

general, the six daytime OA factors collectively explain the majority (82 %) of daytime SOA identified by an aerosol mass spectrometer (AMS). While BB-LVOA and Night-LVOA accounted for 13 % of biomass burning OA and 48 % of nighttime chemistry OA observed by AMS, respectively. Our PMF analysis also demonstrated that the highly oxygenated OA and hydrocarbon-like OA cannot be identified with FIGAERO-CIMS in this study. In summary, our results show that the volatility of OA is strongly governed by its formation pathways and subsequent atmospheric aging processes.

1 Introduction

Secondary organic aerosols (SOA), a major component of fine particulate matter (PM_{2.5}) in China (Zhou et al., 2020), exert profound influences on climate change, human health, and air quality (Arias et al., 2021; Apte et al., 2018; Huang et al., 2014). Despite notable reductions in primary emission in recent years, SOA has emerged as an increasingly crucial factor in haze formation in China (Zhang et al., 2018). However, accurately modeling SOA from current chemical models is still challenging, largely attributed to our limited understanding of its formation mechanisms (Charan et al., 2019; Matsui et al., 2009; Lu et al., 2020). Thus, there is a crucial need for a comprehensive understanding of SOA formation and aging processes in the ambient environment.

Positive matrix factorization (PMF) has been widely used to apportion the contribution of primary and secondary sources to organic aerosol (OA) (Chen et al., 2014, 2021a; Ou et al., 2023; Tian et al., 2016). For the input of OA, the matrix of time serial spectral of OA measured by the Aerodyne Aerosol Mass Spectrometers (AMS) or Aerosol Chemical Speciation Monitor (ACSM) was usually applied (Uchida et al., 2019; Canonaco et al., 2013). Based on this approach, various primary OA (POA) components such as, hydrocarbon-like OA (HOA, associated with traffic emission), biomass burning OA (BBOA), cooking OA (COA), and secondary OA (SOA) with different oxidation levels are broadly identified in field measurements (Zhang et al., 2011; Jimenez et al., 2009; Huang et al., 2010, 2018; Qin et al., 2017; Guo et al., 2020; Al-Naiema et al., 2018). OA factors are generally distinguished according to their features on mass spectral and time series (Ulbrich et al., 2009; Lee et al., 2015). However, the electric ionization sources (70 eV), together with thermal decomposition at 600 °C, lead to strongly fragmented ions detected in AMS/ACSM. These fragmented ions lack parent molecular information, thus hindering the ability to further attribute OA factors to more specific sources, thereby limiting our understanding of SOA formation pathways and aging mechanisms in ambient environments. To overcome this challenge, applying PMF analysis of molecular-level datasets is needed for refining SOA source apportionment. Recently, chemical ionization mass spectrometer coupled with the Filter Inlet for Gases and Aerosols (FIGAERO-CIMS) has been increasingly employed for the molecular-level characterization of

oxygenated organics compounds in the gas and particle phase (Ye et al., 2021; Thornton et al., 2020). Using this approach, Ye et al. (2023) employed PMF analysis to FIGAERO-CIMS data sets and found that low-NO-like pathway had a significant contribution to SOA formation in urban area.

Volatility, an important property of organic compounds, is frequently described as saturation mass concentration (C^* , Donahue et al., 2006). The volatility of organic compounds is closely related to its chemical characteristics, including oxidate state, number of carbons, and functional groups (Donahue et al., 2012, 2011; Ren et al., 2022). The gas–particle partitioning behavior of organic compounds is largely governed by their volatility, and thus strongly influence the formation of SOA (Nie et al., 2022). Moreover, chemical processes occurring in the particle phase can alter the volatility of organic compounds. For example, high molecular weight organic compounds can form through accretion reactions, leading to a reduction in volatility (Barsanti and Pankow, 2004; Jenkin, 2004; Kroll and Seinfeld, 2008). In addition, particle phase organic compounds can be oxidized by atmospheric oxidants (e.g., O₃, OH, and NO₃), which can also alter the chemical characteristic and volatility (Rudich et al., 2007; Walser et al., 2007). Thus, the variation of volatility can provide valuable information about the formation and aging processes of OA. Graham et al. (2023) found that SOA from NO₃ oxidation of α -pinene or isoprene had a higher volatility than it from β -caryophyllene. Hildebrandt Ruiz et al. (2015) demonstrated that exposure to different OH levels could lead to a large variation in SOA volatility.

However, linking OA volatility directly to its chemical characteristics and sources remains challenging. A thermodesigner (TD) coupled with an AMS has been employed to investigate the volatility of OA from different sources (Louvaris et al., 2017). Xu et al. (2021) estimated the volatility of different PMF OA factors in the North China Plain and reported that RH level could alter both the formation pathway and volatility of more oxidized oxygenated OA. Feng et al. (2023) reported the much lower OA volatility from out plumes of North China plain than results obtained in the urban areas, signifying the aging impact on OA volatility. Nevertheless, owing to the operational principle of AMS, it is still difficult to obtain molecular information of organic compounds at different volatilities. In contrast, the FIGAERO-CIMS provides not only molecular-level measurements but also thermal desorption profiles (thermograms) for each de-

ected compound. The temperature of the peak desorption signal (T_{\max}) of a specific compound is typically correlated with its volatility (Lopez-Hilfiker et al., 2014), enabling direct connects between the volatility and organic molecular (Ren et al., 2022). Huang et al. (2019) analysis the ambient particles filter samples collected in different seasons with FIGAERO-CIMS and reported a lower volatility of oxygenated OA in winter, partly due to higher O : C. Buchholz et al. (2020) utilized PMF analysis of FIGAERO-CIMS thermogram data sets to investigate physicochemical property of laboratory-generated SOA particles.

To comprehensively investigate the evolution of OA and its relationship with volatility in ambient environment, we employed a FIGAERO-CIMS along with other online instruments to gain a comprehensive understanding of the variation in SOA volatility within urban plumes in the Pearl River Delta (PRD) region during the fall of 2019. PMF analysis was performed on thermograms data obtained from the FIGAERO-CIMS. By combining the source apportionment of thermogram organic aerosol (OA) with corresponding volatility information, we investigated the potential formation pathway and influencing factors of SOA in the urban downwind region.

2 Measurement and Method

2.1 Field Measurements

We conducted a field campaign at the Heshan supersite in the PRD region from 29 September–17 November 2019. Considering the integrity of the measurements, we focus primarily on the period from 16 October–16 November 2019 in this study. The measurement site was located in a rural area surrounded by farms and villages (at $22^{\circ}42'39.1''$ N, $112^{\circ}55'35.9''$ E, with an altitude of about 40 m), situated to the southwest of the PRD region. All online instruments were placed in air-conditioned rooms on the top floor of the supersite building.

A FIGAERO-CIMS, coupled with an X-ray source, was used to measure organic compounds in both the gas- and particle-phase, utilizing I^- as the chemical ionization reagent. The instrument operated on 1 h cycle by switching between two modes (sampling mode and desorption mode) for measuring gas- and particle-phase oxygenated organic molecules. In the sampling mode, ambient gas was measured in the first 21 min, followed by a 3 min zero air background, while the $\text{PM}_{2.5}$ sample was collected on a PTFE membrane filter for 24 min. Then, the instrument was switched to the desorption mode, in which the collected particles were desorbed using heated N_2 . The temperature of the N_2 was increased from approximately 25–175 °C over a 12 min period, and then held at 175 °C for an additional 24 min. Calibration of a few chemicals was conducted in the laboratory. For the remaining organic species, a voltage scanning method was used to determine their sensitivities (referred to as semi-

quantified species) (Ye et al., 2021; Iyer et al., 2016; Lopez-Hilfiker et al., 2016). The detailed operation settings, data processing, and calibration can be found in Cai et al. (2023) and Ye et al. (2021).

A soot particle aerosol mass spectrometer (SP-AMS, Aerodyne Research, Inc., USA) was used to measure the chemical composition of PM_1 particles, including nitrate, sulfate, ammonium, chloride, black carbon, and OA. More details on the quantification using ionization efficiency, composition dependent collection efficiency, data analysis, and source apportionment of OA from AMS data (defined as AMS-OA) could be found in Kuang et al. (2021) and Cai et al. (2024). In brief, AMS-OA consisted of two primary OA factors and four secondary OA factors. The primary OA factors include hydrocarbon-like OA (HOA, 11 %) and biomass burning OA (BBOA, 20 %), which were mainly contributed by traffic and cooking emissions and biomass burning combustion, respectively. For SOA factors, biomass burning SOA (BBSOA, 17 %) was likely formed through oxidation of biomass burning emission; less oxidized oxygenated OA (LO-OOA, 24 %), which results from strong daytime photochemical processes; more oxidized oxygenated OA (MO-OOA, 17 %), related to regional transport; and nighttime-formed OA (Night-OA, 11 %) which was associated with nighttime chemistry.

Trace gases such as O_3 and NO_x were measured by gas analyzers (model 49i and 42i, Thermo Scientific, US). Meteorological parameters, including wind speed and wind direction, were measured by a weather station (Vantage Pro 2, Davis Instruments Co., US).

2.2 Methodology

Positive matrix factorization (PMF) is a widely used tool for source apportionment of long timeseries data (Paatero and Tapper, 1994). In the desorption mode, the particulate organic compounds are thermo-desorbed and simultaneously measured by the FIGAERO-CIMS. Organic molecules with different volatility were characterized by thermograms (desorption signals vs temperature of N_2). Here, we performed PMF analysis to the thermogram data of organic compounds measured by the FIGAERO-CIMS (FIGAERO-OA) using the Igor-based PMF Evaluation Tool (PET, v3.01, Ulbrich et al., 2009), which can be expressed as follows:

$$\mathbf{X} = \mathbf{GF} + \mathbf{E}, \quad (1)$$

where \mathbf{X} is the thermogram organic compound data measured by the FIGAERO-CIMS, which can be decomposed into two matrices \mathbf{G} and \mathbf{F} . The matrix \mathbf{G} , \mathbf{F} , and \mathbf{E} contain the factor time series, factor mass spectra, and the residuals between the measured data and the reconstructed data.

The raw normalized count per second (NCPS) thermogram data with a time resolution of 1 s was averaged to a 20 s-time grid, and then was background-corrected by subtracting linearly interpolated background thermogram sig-

nals. For each scan, only the data points when the desorption temperature increased were used as input data (corresponding to 25–170 °C, 1–70 data points in this study, Fig. S1 in the Supplement), since the main information lies during the species desorbing from the FIGAERO filter (Fig. S1, Buchholz et al., 2020). Then, we combined data from separate thermogram scans (without background scans) to a larger input data set.

To perform the PMF analysis, a data uncertainty matrix ($S_{i,j}$) is needed, where the i and j represents the index of ions and data points, respectively. According to Buchholz et al. (2020), the uncertainty was assumed to be constant for each individual thermogram scan (constant error scheme). The $S_{i,j}$ of a specific thermogram scan can be determined by the following equation:

$$S_{i,j} = \sigma. \quad (2)$$

For each thermogram scan, the last 20 data points are assumed to be in steady state. Thus, the σ_{noise} was calculated as the median of the standard deviation (SD) of the residual ($\text{res}_{i,j}$), which can be obtained from the difference between the data points ($\text{Data}_{i,j}$) and the corresponding linear fitted value ($\text{FittedData}_{i,j}$) for the measured data points (Fig. S2):

$$\text{res}_{i,j} = \text{Data}_{i,j} - \text{FittedData}_{i,j}, \quad (3)$$

$$\sigma = \text{median}(\text{SD}(\text{res}_{i,j})). \quad (4)$$

Due to the large volume of the data matrix ($59\,500 \times 1028$) exceeding the processing capacity of the PET, we had to divide the data matrix into three parts and performed PMF analysis separately. An eight-factor solution was selected for each part based on Q/Q_{exp} behavior and factor interpretability (Figs. S3–S6). To assess factor consistency, the mass spectra of resolved factors were compared across different parts, showing strong correlations ($R > 0.9$) for the each factor (Figs. S7 and S8). Weaker correlations during the early campaign period (2–5 October) likely reflect changes in dominant OA sources under different meteorological conditions (Figs. S8 and S9). After excluding this period, consistent factor profiles were obtained and combined for further analysis. Detailed evaluations are provided in the Sect. S1 in the Supplement.

Since input data sets of PMF analysis were the NCPS data, the signal of each thermograms factor was a combination of NCPS values of different ions. Thus, it is necessary to convert the signal of these factors into mass concentrations, which would increase the representativeness of the thermogram PMF results. The NCPS of a specific ion was linearly correlated with the corresponding mass concentration. Thus, for a signal running cycle (a thermogram scan), the mass concentration of a specific thermograms OA factor k (M_k) can be estimated as:

$$M_k = \sum_i \left(\frac{\sum_j \text{Signal}_{j,k} \times \text{Profile}_{i,k}}{\sum_j \text{NCPS}_{j,i}} \times m_i \right), \quad (5)$$

where i and j represent the index of species and data points; the $\text{Signal}_{j,k}$ is the signal of a thermograms OA factor k at a data index j ; the $\text{Profile}_{i,k}$ represents the fraction of signal of factor k and ion i ; the $\text{NCPS}_{j,i}$ is the NCPS of species i at a data index j ; and m_i is the mass concentration of species i in the particle-phase measured by the FIGAERO-CIMS.

For a specific organic compound, the temperature of the peak desorption signal (T_{max}) has a nearly linear relationship with the logarithm of saturation vapor pressure (P_{sat}) of the respective organic compound (Lopez-Hilfiker et al., 2014):

$$\ln(P_{\text{sat}}) = aT_{\text{max}} + b, \quad (6)$$

where a and b are fitting coefficients. P_{sat} can be converted to saturation vapor concentration (C^* , $\mu\text{g m}^{-3}$) by following equation:

$$C^* = \frac{P_{\text{sat}} M_w}{RT} 10^6, \quad (7)$$

where M_w is the average molecular weight of the organic compound (determined by the FIGAERO-CIMS), R is the gas constant ($8.314 \text{ J mol}^{-1} \text{ K}^{-1}$), and T is the thermodynamic temperature (298.15 K). The fitting parameters of a and b were calibrated by a series of polyethylene glycol (PEG 5–8) compounds before the campaign. PEG standards (dissolved in acetonitrile) were atomized using a homemade atomizer, and the resulting particles were size-classified by a differential mobility analyzer (DMA; model 3081L, TSI Inc.) to target diameters of 100 and 200 nm. The size-selected particles were then split into two flows: one directed go to a CPC (3775, TSI) for the measurements of number concentration, and the other to the FIGAERO-CIMS particle inlet. The collected mass by CIMS was calculated based on the particle diameter, number concentration, FIGAERO-CIMS inlet flow rate, and collection time. The details of the calibration experiments and selection of fitting coefficients (a and b) can be found in Table S1 in the Supplement and Cai et al. (2024). In this study, the fitting parameters ($a = -0.206$ and $b = 3.732$) were chosen, as the mass loading (407 ng) and diameter (200 nm) are closest to the ambient samples, since the collected mass loading centered at about 620 ng and the particle volume size distribution (PVSD) centered at about 400 nm (Cai et al., 2024). It was worth noting that the volatility range of PEG 5–8 ($-1.73 \leq \log_{10} C^* \leq 3.34 \mu\text{g m}^{-3}$) may not fully represent the volatility of ambient organic aerosol, particularly nitrogen-containing and highly oxygenated compounds that can exhibit much lower volatility ($\log_{10} C^* \leq -2 \mu\text{g m}^{-3}$, Ren et al., 2022; Chen et al., 2024). At present, saturation vapor pressure data for PEG standards are only available up to PEG-8 (Krieger et al., 2018). Ylisirniö et al. (2021) demonstrated that different extrapolation approaches for estimating the volatility of higher-order PEGs can lead to substantial discrepancies in calibration results, and they strongly recommended that higher-order PEGs should only be used to extend the volatility calibration range once their

saturation vapor pressures are accurately determined. Very recently, Ylisirniö et al. (2025) derived saturation vapor pressures for higher-order PEGs up to PEG-15 and demonstrated that extending FIGAERO-CIMS calibration to much lower volatilities is feasible, but also showed that different estimation approaches for higher-order PEGs can lead to large discrepancies, highlighting substantial uncertainties when extrapolating volatility calibration beyond PEG-8. Therefore, uncertainties may remain in the calibration of low-volatility OA, and further calibration experiments using complementary techniques are highly recommended. Therefore, uncertainties may remain in the calibration of low-volatility OA, and further calibration experiments using complementary techniques are highly recommended.

3 Results

3.1 Overview of FIGAERO-OA factors

In this study, the average mass concentration of FIGAERO-OA was about $5.3 \pm 2.4 \mu\text{g m}^{-3}$. The thermogram data sets of FIGAERO-OA were analyzed with PMF and mass concentration of each factor was estimated based on Eq. (5), which provide volatility and mass concentration information of OA originating from different formation pathways. An 8-factor solution was chosen to explain the thermogram of FIGAERO-OA. These factors included six associated with daytime photochemical reactions, one related to biomass-burning, and one factor contributed by nighttime chemistry. The diurnal variation, mass spectra, and thermograms of these factors can be found in Fig. S9. The estimated volatility ($\log_{10} C^*$), T_{\max} , and elemental information of all factors are shown in Table 1. Given that the thermogram data can provide volatility information of organic compounds, the identified OA factors were categorized based on their potential formation pathway, volatility, and correlation with AMS PMF factors (Table 1 and Fig. S10). For example, if the PMF factor with a T_{\max} located in the ranges of low volatile organic compounds (LVOC, approximately corresponding to 78.8–112.3 °C then Fig. 1), this factor will be named after low volatility OA (LVOA). For the factors whose T_{\max} is above 112.3 °C, extremely low volatility (ELVOA) will be named.

The six daytime chemistry related factors include a low volatility OA factor likely formed under high NO_x condition (Day-HNO_x-LVOA, 12 %), a low volatility factor contributed by gas-particle partitioning (Day-LNO_x-LVOA, 11 %), a low volatility and an extremely low volatility factor originating from the daytime aging process (Day-aged-LVOA and Day-aged-ELVOA, 16 % and 11 % respectively), and a low volatility and an extremely low volatility factors related to urban air masses (Day-urban-LVOA and Day-urban-ELVOA, 16 % and 7 %, respectively). These daytime factors accounted for about 76.4 % of the total mass of FIGAERO-OA and demonstrated distinct daytime peak. The total mass of daytime FIGAERO-OA factors showed a strong positive

correlation with LO-OOA in AMS-OA ($R = 0.86$), which was attributed to photochemical reactions (Fig. S10a).

Both Day-HNO_x-LVOA and Day-LNO_x-LVOA reached their peak values at about 14:00 LT (Fig. 1a1 and b1), implying strong photochemical production. Day-HNO_x-LVOA had the highest N:C (0.06) and the lowest oxidation state ($\text{OS}_c = -0.01$), which could be attributed to the “high NO_x ” formation pathway. It was also supported by significant positive correlation ($R = 0.93 - 0.94$) with particulate phase nitrogen-containing organic compounds (e.g., C₄H₅NO₆, C₈H₁₁NO₈, and C₈H₁₁NO₉). Previous studies found that high NO_x concentration can suppress the production of molecules with a high oxidation degree (Rissanen, 2018; Praske et al., 2018), which could explain the low OS_c value (-0.01) and relative high volatility ($\log_{10} C^* = -0.98$) found for Day-HNO_x-LVOA. Day-LNO_x-LVOA had a higher OS_c (0.18) and lower $\log_{10} C^*$ (-2.71) than Day-HNO_x-LVOA, consistent with that Day-LNO_x-LVOA was composed of smaller and more oxidized non-nitrogen containing compounds (e.g., C₂H₂O₃, C₃H₄O₃, C₄H₆O₄, and C₆H₈O₄). Noting that C₂–C₃ group could originate from the decomposition of larger molecules during thermal desorption, since the thermogram of C₂H₂O₃ and C₃H₄O₃ demonstrated a bimodal distribution (Fig. 9a). Figure S12b and d further examine the contribution of all FIGAERO factors to the signals of C₂H₂O₃ and C₃H₄O₃. One mode, peaking in the LVOC range, was primarily associated with Day-LNO_x-LVOA, and a second mode, peaking in the ELVOC range, was dominated by Day-aged-ELVOA. These results indicates that these two low molecular weight species are likely decomposition products of at least two distinct classes of higher molecular weight organic compounds.

Additionally, we identified two aged OA factors (Day-aged-LVOA and Day-aged-ELVOA) with an afternoon peak at about 18:00 LT (Fig. 1c1 and d1), which may be derived from the aging transformation of preexisting organic aerosols via daytime photochemical reactions. These aged factors exhibited the highest OS_c (0.35 and 0.40) and relatively low volatility with a $\log_{10} C^*$ of -2.02 and -4.80 , respectively. Day-aged-LVOA was featured with a series of C₄–C₈ oxygenated compounds (e.g., C₄H₆O₅, C₅H₈O₅, C₆H₁₀O₅, C₇H₁₀O₅, and C₈H₁₂O₅). In contrast, Day-aged-ELVOA had a higher fraction of smaller molecules (e.g., C₂H₄O₃ and C₃H₆O₃, Fig. 1d2). Chen et al. (2021b) found that low molecular weight carboxylic acids (LMWCA) could form through SOA aging processes and report a strong correlation ($R^2 = 0.90$) between LMWCA and highly oxygenated OA. However, C₂H₄O₃ and C₃H₆O₃ had a weak correlation ($R = 0.49$ and 0.13) with MO-OOA resolved from AMS (Fig. S11). In addition, the T_{\max} of C₂H₄O₃ and C₃H₆O₃ located in the ELVOC range and showed thermogram profiles similar to that of Day-aged-ELVOA (Fig. S12a). The thermogram signal of C₂H₄O₃ and C₃H₆O₃ was mainly contributed by Day-aged-ELVOA (Fig. S12c and e), supporting the interpretation that these species are more likely decomposition

Table 1. The average volatility ($\log_{10} \overline{C^*}$), T_{\max} , signal-weighted average values of elemental composition, carbon oxidation state (\overline{OS}_c), H : C, O : C, N : C for all FIGAERO-OA factors. The estimation of \overline{OS}_c can be found in Sect. S2. The volatility of each FIGAERO-OA factor was estimated based on their corresponding T_{\max} using Eqs. (8) and (9).

	$\log_{10} \overline{C^*}$ ($\mu\text{g m}^{-3}$)	T_{\max} ($^{\circ}\text{C}$)	Average elemental composition	\overline{OS}_c	H : C	O : C	N : C
Day-HNO _x -LVOA	-0.98	84.52	C _{7.37} H _{10.51} O _{4.99} N _{0.36}	-0.01	1.37	0.75	0.06
Day-LNO _x -LVOA	-2.71	103.29	C _{6.52} H _{8.77} O _{4.54} N _{0.22}	0.18	1.35	0.80	0.04
Day-aged-LVOA	-2.02	95.53	C _{6.35} H _{8.75} O _{5.13} N _{0.21}	0.35	1.42	0.91	0.04
Day-aged-ELVOA	-4.80	126.65	C _{5.22} H _{7.36} O _{4.20} N _{0.16}	0.40	1.55	1.00	0.03
Day-urban-LVOA	-0.90	83.03	C _{6.50} H _{9.27} O _{4.71} N _{0.24}	0.08	1.43	0.80	0.04
Day-urban-ELVOA	-7.18	153.22	C _{6.57} H _{8.54} O _{4.61} N _{0.24}	0.26	1.35	0.84	0.05
BB-LVOA	-2.36	99.39	C _{6.72} H _{9.78} O _{4.61} N _{0.26}	-0.08	1.47	0.74	0.04
Night-LVOA	-2.02	95.53	C _{7.69} H _{11.04} O _{5.19} N _{0.47}	-0.09	1.47	0.77	0.07

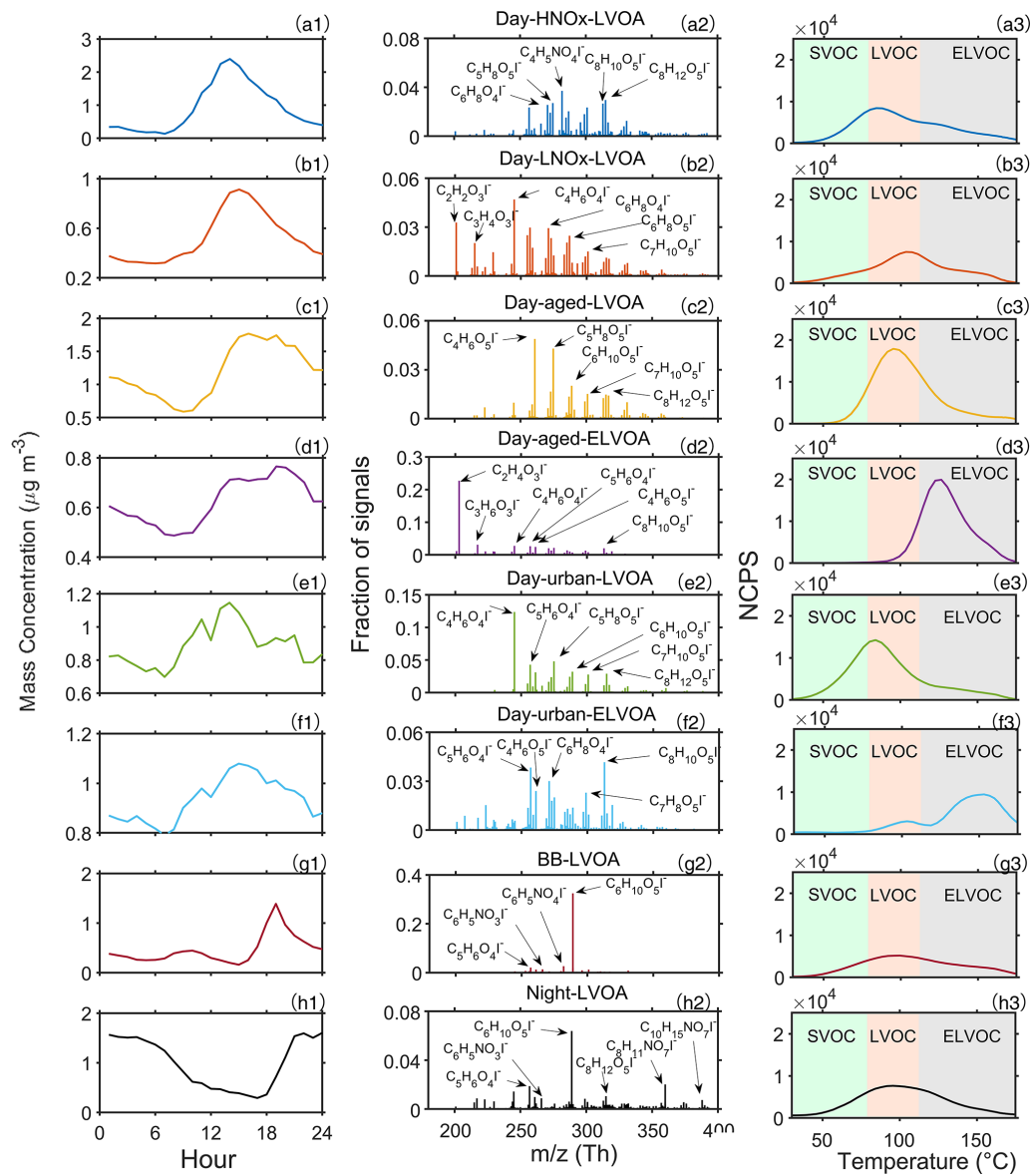


Figure 1. Diurnal variation (a1–h1), mass spectra (a2–h2), and thermograms (a3–h3) of FIGAERO-OA factors.

products of low volatility organic compounds rather than being directly formed through atmospheric aging processes.

Two urban air masses-related OA factors (Day-urban-LVOA and Day-urban-ELVOA) were identified, which would be discussed in the following section. Day-urban-LVOA demonstrated comparable \overline{OS}_c (0.08), O : C (0.80) and volatility (−0.90) to Day- HNO_x -LVOA (−0.01, 0.75, and −0.98, respectively), but show a higher fraction of non-N-containing molecules (e.g., $C_4H_6O_4$, $C_5H_6O_4$, $C_5H_8O_5$, and $C_7H_{10}O_5$) and a reduced N : C ratio (Table 1). However, the oxidation state (\overline{OS}_c) of Day- HNO_x -LVOA (−0.01) was significantly lower than that of Urban-LVOA (0.08), accompanied by a relatively higher N : C (0.06 vs. 0.04). Despite its lower oxidation state, the volatility of Day- HNO_x -LVOA is comparable to that of Day-urban-LVOA, which may reflect differences in functional group composition. For example, a nitrate group (− ONO_2) contributes to volatility reduction at a level comparable to that of a hydroxyl group (−OH) and generally more strongly than carbonyl functionalities such as aldehydes (− $C(O)H$) or ketones (− $C(O)−$) (Pankow and Asher, 2008). However, due to instrumental limitations, we are unable to directly resolve the functional group composition of individual OA factors, and further measurements employing new techniques are needed to better constrain the role of functional groups in controlling the volatility of ambient organic aerosol. Day-urban-ELVOA had the lowest volatility ($\log_{10}C^* = -7.18$) but an \overline{OS}_c (0.27) lower than Day-aged-ELVOA (0.34) and composed of oxygenated compounds (e.g., $C_8H_{10}O_5$, $C_7H_8O_5$, $C_6H_8O_4$, and $C_5H_6O_4$). The thermogram of Day-aged-ELVOA demonstrates bimodal distribution (peaked at LVOC and ELVOC range) and had a highest T_{max} (153.2 °C) among thermograms OA factors (Fig. 1f3). However, the majority of organic molecules (e.g., $C_5H_6O_4$, $C_4H_6O_5$, $C_6H_8O_4$, and $C_8H_{10}O_5$) do not exhibit thermograms similar to that of Day-urban-ELVOA (Fig. S13). Instead, their thermograms demonstrate multimodal distributions and are contributed by multiple FIGAERO factors. For example, a mode of $C_5H_6O_4$ peaking in the LVOC range was mainly contributed by Day-urban-LVOA, while two modes peaking in the ELVOC range were primarily contributed by Day-aged-ELVOA and Day-urban-ELVOA, respectively. These results suggest that these molecules may originate from both direct desorption of organic aerosol and thermal decomposition of higher-molecular-weight compounds during heating.

The biomass-burning related factor, biomass-burning less volatile organic aerosol (BB-LVOA, 10 % of FIGAERO-OA), had a low \overline{OS}_c (−0.07), the lowest O : C (0.74), and positive correlation with BBOA resolved from AMS ($R = 0.64$, Fig. S10b). It presented a prominent peak at 19:00 LT and was identified by the distinctive tracer levoglucosan ($C_6H_{10}O_5$), nitrocatechol ($C_6H_5NO_4$), and nitrophenol ($C_6H_5NO_3$, Fig. 1) in the spectrum, which was frequently detected in biomass burning plumes (Gaston et al., 2016; Ye et al., 2021). In the upwind urban region of Heshan site, Ye

et al. (2023) identified a biomass burning related factor in Guangzhou city using the FIGAERO-CIMS, with a distinct evening peak at 21:00 LT and more abundance oxygenated compounds (e.g., $C_7H_{10}O_5$ and $C_8H_{12}O_6$). The different oxidation level of BBOA between Guangzhou and Heshan, suggest the BB-LVOA in this study is more related to the direct BB emission, but the BB factor in Guangzhou is more resembled BB related SOA factor. This statement was supported by the fact that biomass burning activities were frequently observed near the measurement site during this study, while the biomass burning activities in urban areas was prohibited and can be transported from nearby suburban agricultural areas (Cai et al., 2023).

The nighttime chemistry related less volatile OA (Night-OA, 15 % of FIGAERO-OA) has the highest N : C (0.07) and exhibited an enhanced at nighttime (22:00–24:00 LT, Fig. 1). Notably, this nighttime factor was composed of a series of organic nitrates (e.g., $C_8H_{11}NO_7$, and $C_{10}H_{15}NO_7$), which was related to the products from monoterpenes oxidized by the NO_3 radical or oxidation of biomass burning products during nighttime (Faxon et al., 2018; Decker et al., 2019). Noting that the levoglucosan ($C_6H_{10}O_5$) was also abundant in the Night-LVOA, suggesting that part of this factor could be attributed to the nighttime aging process of biomass burning products (Jorga et al., 2021). The detailed discussion about the potential formation pathway of these six daytime FIGAERO-OA factors will be discussed in Sect. 3.2.

The volatility of organic compounds was closely related to their chemical characteristics (Donahue et al., 2012). Figure 2 demonstrates the relationship between $\log_{10}\overline{C}^*$ of thermogram factors and \overline{OS}_c , O : C, and number of carbons (nC). In general, these factors exhibited a negative correlation ($R = -0.60$ and -0.73) with both the \overline{OS}_c and the O : C but showed a positive correlation ($R = 0.73$) with nC (Fig. 2), except for Day-urban-ELVOA. As aforementioned, the major component of Day-urban-ELVOA could be decomposition products of larger oxygenated molecules. Thus, the chemical characteristic of Day-urban-ELVOA did not demonstrate a similar relationship of volatility versus molecule indicators (e.g., oxidation state, O : C and nC) as other factors. The increase of carbon number usually lead to a decrease in volatility (Donahue et al., 2011), while this trend overturned in this campaign (Fig. 2c). Figure 2d shows that \overline{OS}_c had a negative relationship ($R = -0.84$) with carbon number, suggesting that organic factors with a higher oxidation degree had a shorted carbon backbone. It could be partly owing to fragmentation of organic molecules during aging processes (Chacon-Madrid and Donahue, 2011; Jimenez et al., 2009). Consistently, two aged factors (Day-aged-LVOA and Day-aged-ELVOA) had a higher \overline{OS}_c and a lower carbon number than other factors. Additionally, it indicates that the increase in oxidation degree outweighed the effect of decreasing nC , leading to a reduction in the volatility of OA during this campaign.

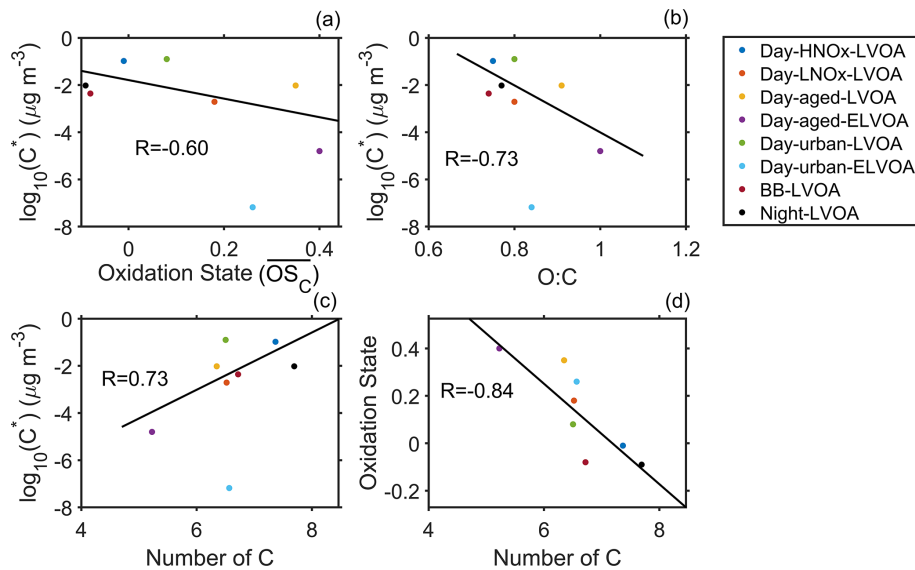


Figure 2. The average volatility of FIGAERO-OA factor vs. (a) oxidation state (\overline{OS}_C), (b) O:C, and (c) number of carbons and (d) number of carbons vs. \overline{OS}_C of thermogram factor. Day-urban-ELVOA is excluded in the estimation of R .

The temporal variation of volatility distribution and mean C^* of FIGAERO-OA, the sum of six daytime factors in FIGAERO-OA and LOOA in AMS OA, mass fraction of eight FIGAERO-OA factors, and wind direction and speed are demonstrated in Fig. 3. As shown in Fig. 3, the increase of mean C^* during the daytime (6:00–18:00 LT, Fig. S14a) is usually accompanied by the enhancement of daytime factors in FIGAERO-OA and LO-OOA from AMS (Fig. S14b and c), indicating that the formation of these factors could notably increase OA volatility. Notably, FIGAERO-OA with a $\log_{10}C^*$ of $-1 \mu\text{g m}^{-3}$ showed pronounced enhancements during the increasing of mean C^* , implying that the volatility of six daytime factors might cluster around $10^{-1} \mu\text{g m}^{-3}$ (Fig. S14d). In Fig. 3b, distinct diurnal variation of O_x ($O_x = O_3 + NO_2$) was observed during the campaign. The maximum of O_x can be as high as $230 \mu\text{g m}^{-3}$, highlighting strong photochemical reaction. The daytime factors, especially Day-HNO_x-LVOA (Fig. 3c), exhibited markable enhancements under weak northwesterly to northeasterly wind (Figs. 3d and S15). A backward trajectory analysis revealed that the measurement site was mainly affected by the urban pollutants from the city cluster around Guangzhou (Fig. S16). Two periods, which were long-range transport and urban air masses periods, respectively, were selected to further analyze the impact of urban pollutants on the formation and aging process of OA. The variation of OA volatility based on wind direction and speed, together with backward trajectory analysis, were also explored (Fig. S16 and Table S2). In general, during the urban air masses period, the site was influenced by regional urban plumes from the northeast city cluster, while the long-range transport period was primarily associated with air masses advected from the north-

east inland regions. More detailed discussion will be shown in the following section.

3.2 Potential formation pathway of FIGAERO-OA

Figure 4 demonstrates distinct differences in the diurnal variation of thermograms factors (including Day-HNO_x-LVOA, Day-aged-LVOA, Day-urban-LVOA, and Day-urban-ELVOA) during long-range transport period and urban air masses period. During the urban air masses period, Day-HNO_x-LVOA significantly increased from ~ 0.4 to $\sim 4.8 \mu\text{g m}^{-3}$ in the daytime. The mass concentration of Day-urban-LVOA and Day-urban-ELVOA demonstrated daytime enhancements only during urban period, suggesting that the formation of these factors was closely related to the pollutants in the urban plumes. Consistently, During the urban air masses period, the maximum ozone concentration in the afternoon (12:00–18:00 LT, $208.3 \mu\text{g m}^{-3}$) was higher than that ($185.5 \mu\text{g m}^{-3}$) during long-range transport period, indicating a stronger photochemical reaction in the urban plumes (Fig. 4). Thus, the daytime thermogram factors accounted for a higher fraction (79 % vs. 75 %) of FIGAERO-OA (Fig. S17). Additionally, the average mass concentration of all thermogram factors ($8.9 \pm 5.1 \mu\text{g m}^{-3}$) was noticeably increased compared to the long-range period ($5.3 \pm 2.4 \mu\text{g m}^{-3}$). Elevated NO_x concentration was observed in the urban plumes in the afternoon (12:00–18:00 LT, 17.4 ppbv vs. 11.7 ppbv), which might also affect the formation pathway of SOA. Both NO and NO/NO₂ remained at a relative low level (0.6–0.8 ppbv and < 0.5) in the afternoon during these two periods (Fig. S18), suggesting an important role of low-NO-like pathway (Ye et al., 2023). Nihill et al. (2021) found that the production of OH and oxidized or-

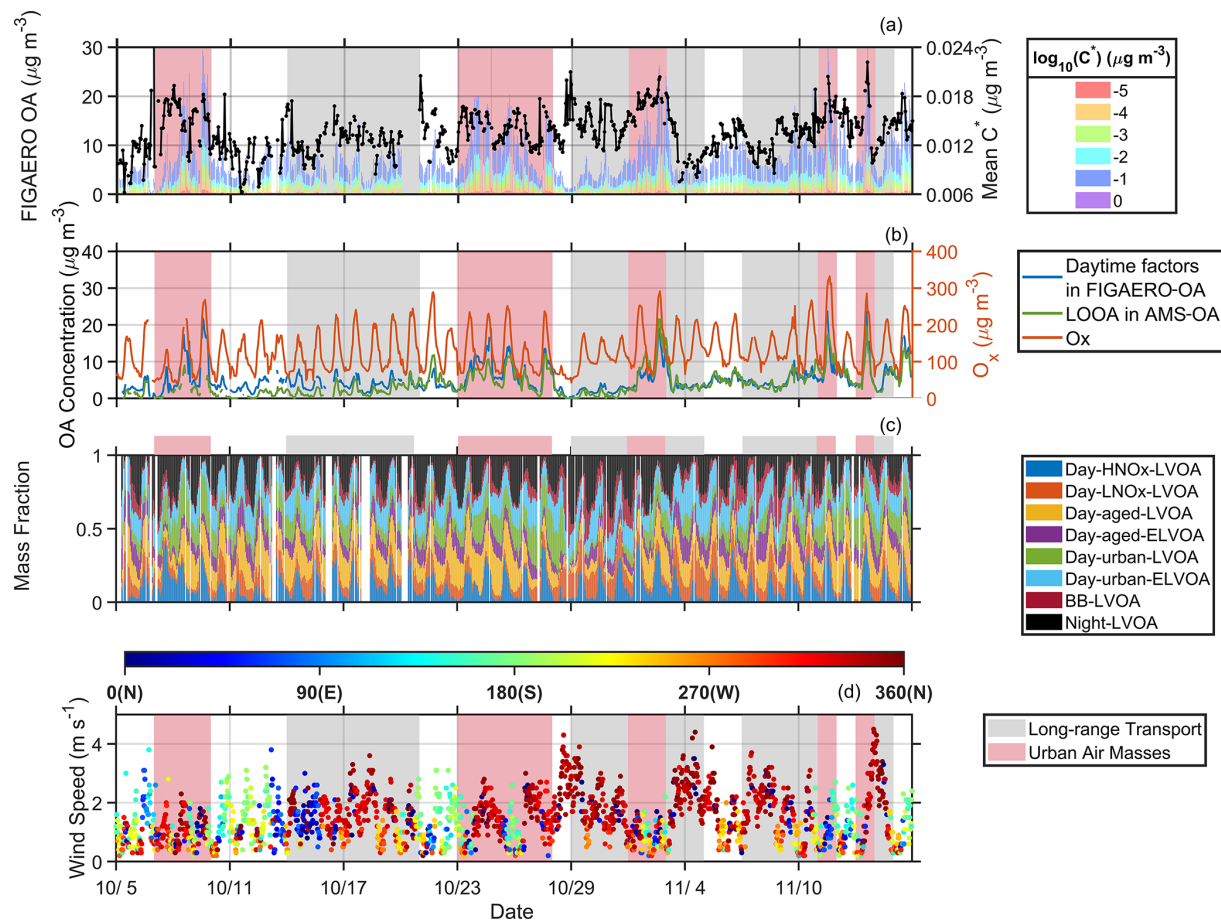


Figure 3. Time series of (a) volatility (presented in a range from $10^{-5} - 10^0 \mu\text{g m}^{-3}$) of FIGAERO-OA and mean C^* , (b) daytime factors (Day-HNO_x-LVOA, Day-LNO_x-LVOA, Day-aged-LVOA, Day-aged-ELVOA, Urban LVOA, and Day-urban-ELVOA) in FIGAERO-OA and LOOA factor from PMF analysis of SP-AMS data, (c) mass fraction of eight FIGAERO-OA factors, and (d) wind speed and wind direction.

ganic molecules would be suppressed under high NO/NO₂ (> 1) condition. Notably, Day-HNO_x-LVOA accounted for the largest portion (29 %) of FIGAERO-OA in the afternoon (12:00–18:00 LT, Fig. S19), followed by Day-aged-LVOA (21 %), while Day-LNO_x-LVOA contributed only 6 %. In contrast, during the long-range transport period, the mass fraction of Day-LNO_x-LVOA significantly increased (from 6 % to 15 %) along with a decrease in Day-HNO_x-LVOA (from 29 %–21 %). These results indicate that elevated NO_x concentration in urban plumes might alter the formation pathway of SOA (Cai et al., 2024). Note that the sum of six daytime FIGAERO factors showed a positive relationship ($R = 0.80$ and 0.76, respectively) with LOOA during both periods (Fig. S20). However, the slope (0.81) of the linear regression during the urban air masses period was higher than that (0.58) during the long-range transport period, indicating that a higher fraction of LOOA could be detected by the FIGAERO-CIMS during urban air masses period. This difference could be related to the discrepancy in OA volatil-

ity. According to Cai et al. (2024), the volatility of OA was higher during the urban air masses period.

To explore the potential formation pathway of daytime factors, Fig. 5 demonstrates the variation of mass concentrations of six daytime factors as a function of O_x, total gas-phase organic molecules measured by the FIGAERO-CIMS (referred as organic vapors), and NO₃⁻/SIA. Five factors, excluding Day-urban-LVOA, exhibited positive correlations with O_x, highlighting the critical role of photochemical reactions in their formation. Previous studies have demonstrated that gas-particle partitioning plays a key role in SOA formation (Nie et al., 2022; Wang et al., 2022). In this study, organic vapors had strong positive correlations with Day-HNO_x-LVOA ($R = 0.73$) and Day-LNO_x-LVOA ($R = 0.74$), suggesting that these factors were mainly formed via gas-particle partitioning. The median concentration of Day-HNO_x-LVOA dramatically increased (from ~ 0 to $\sim 5.6 \mu\text{g m}^{-3}$) with rising organic vapors, whereas a comparable enhancement was not observed for Day-LNO_x-LVOA (Fig. 5b1 and b2).

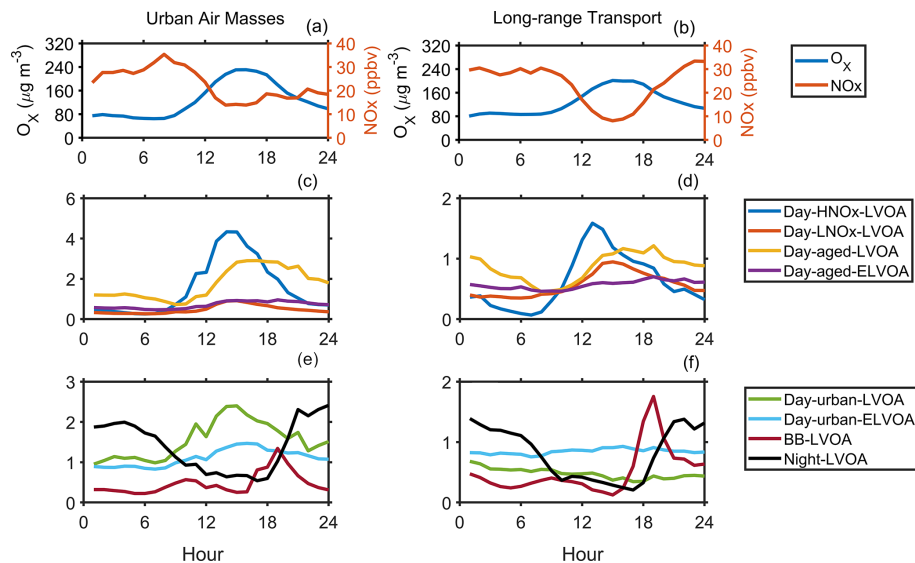


Figure 4. The average diurnal variation of O_X , NO_X , and mass concentration of eight thermogram factors during the long-range transport (**a, c, e**) and urban air masses (**b, d, f**) period.

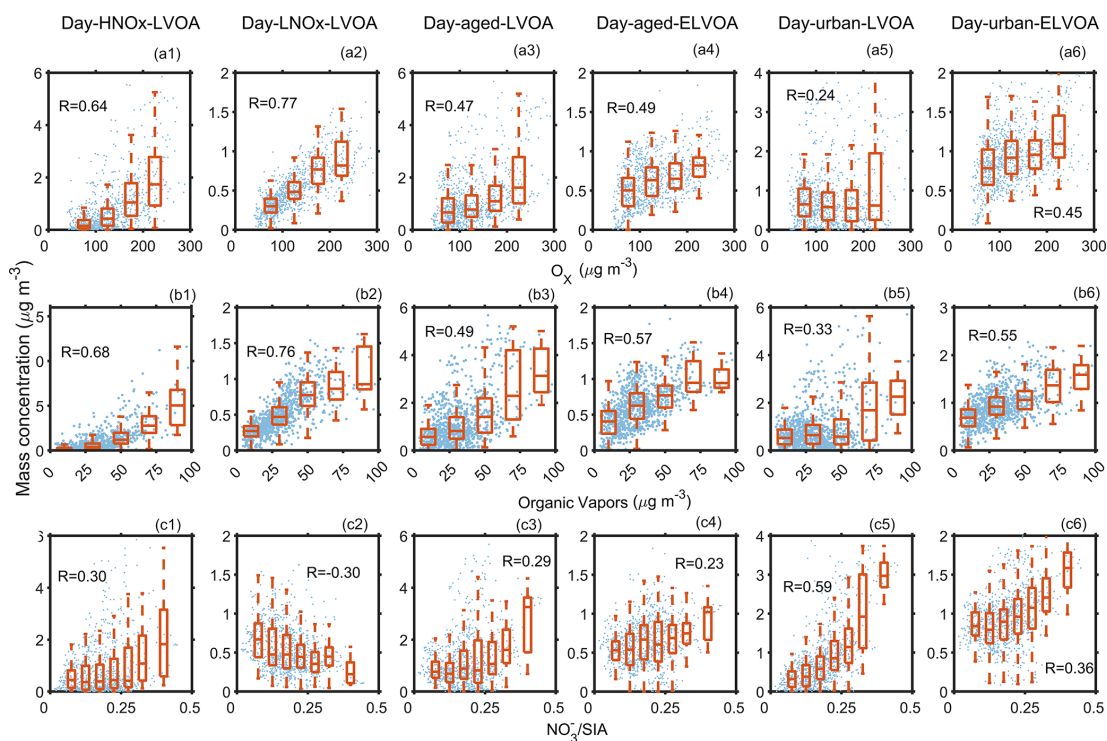


Figure 5. Relationship between the mass concentration of six daytime thermogram factors and (**a1-a6**) O_X , (**b1-b6**) organic vapors, (**c1-c6**) nitrate fraction in secondary inorganic aerosol (SIA), and (**d1-d6**) sulfate fraction in SIA measured by the FIGAERO-CIMS. The organic vapors are the sum of organic compounds in the gas-phase measured by the FIGAERO-CIMS.

Furthermore, NO_X impact on Day-HNO_x-LVOA and Day-HNO_x-LVOA was investigated here. Figure S21 show Day-HNO_x-LVOA concentrations were consistently higher under elevated NO_X conditions, while Day-HNO_x-LVOA decreased with increasing NO_X level. Figure 6a displays the

mass ratio of Day-HNO_x-LVOA to Day-LNO_x-LVOA obviously increased with organic vapors (up to 12–26) under high NO_X condition (> 20 ppbv), while the ratio remained at approximately 2 at low NO_X level (< 10 ppbv). These overall results suggest that Day-HNO_x-LVOA forma-

tion was predominantly governed by gas-particle partitioning under high NO_x condition, which were typically sustained during urban air masses period (Fig. 2d). Figure 6b compares the relative mass fraction of molecular composition in two gas-particle partitioning related factors, Day- HNO_x -LVOA and Day- LNO_x -LVOA. The mass fraction of species was derived from the signal profile of corresponding factors based on their sensitivity (Ye et al., 2021). Day- HNO_x -LVOA presented greater proportions (10^{-5} – 10^{-3}) of organic nitrates (ONs) than Day- LNO_x -LVOA (10^{-11} – 10^{-9}), including $\text{C}_4\text{H}_7\text{NO}_6$, $\text{C}_8\text{H}_9\text{NO}_4$, $\text{C}_8\text{H}_{11}\text{NO}_7$, as well as nitrophenols (e.g., $\text{C}_7\text{H}_7\text{NO}_3$), which are characterized by relatively low $\overline{\text{OS}}_{\text{C}}$. These compounds were probably attributed to the SOA formation under elevated NO_x concentration (Fig. 2d). In contrast, Day- LNO_x -LVOA was enriched in non-nitrogen-containing species (e.g., $\text{C}_4\text{H}_6\text{O}_3$, $\text{C}_5\text{H}_{10}\text{O}_3$, $\text{C}_{11}\text{H}_{17}\text{O}_6$), which exhibited a higher $\overline{\text{OS}}_{\text{C}}$. These results indicate that NO_x exerts contrasting effects on the formation of these two gas-particle partitioning-related factors.

Previous studies show that NO_x has a nonlinear effect on the formation of highly oxygenated organic (HOM) compounds by influencing the atmospheric oxidation capacity and RO_2 autoxidation (Xu et al., 2025; Pye et al., 2019; Shrivastava et al., 2019). NO_x could suppress the production of low-volatility molecules by inhibiting autoxidation (Rissanen, 2018; Praske et al., 2018), while Nie et al. (2023) found that NO could enhance the formation of HOM at low NO condition (< 82 pptv). During this campaign, the average NO_x and NO was about 24.0 and 2.3 ppbv, respectively, substantially higher than the “low-NO-regime” described by Nie et al. (2023). Our previous study reported a lower concentration of organic vapors with a high $\overline{\text{OS}}_{\text{C}}$ within urban plumes during the same campaign (Cai et al., 2024). We investigate diurnal evolution of organic compositions under long-range transport and urban air masses periods (Fig. S22). Mass concentrations of CHON increase during the daytime in both periods, with a more pronounced enhancement observed in urban air masses (Fig. S22a). However, the mass fraction of CHON was lower during the urban air masses period than during the long-range transport period. We speculated that elevated NO_x enhances overall oxidation and product formation rather than selectively enriching nitrogen-containing compounds. This interpretation is consistent with results from our previous observation-constrained box-model simulations, in which production rates of OH and organic peroxy radicals (RO_2) were evaluated under varying NO_x and VOC conditions (Cai et al., 2024). The modeled $P(\text{OH})$ were close to the transition regime, indicating that elevated NO_x can enhance atmospheric oxidation capacity. In contrast, the $P(\text{RO}_2)$ was in the VOC-limited regime and decreased with increasing NO_x . Consistent with these results, Fig. S22c shows that the mass fraction of highly oxygenated organic molecules ($\text{O} \geq 6$) is lower during urban air masses period. Concurrently, species with low oxygen numbers ($\text{O} \leq 3$) become relatively more abundant in the urban plumes

(Fig. S22c), indicating a shift in the oxidation product distribution toward less oxygenated and potentially more volatile compounds, the NO_x -driven suppression of multigenerational autoxidation inferred from the box-model results. This suppression of oxidation is observed for both CHON and CHO species. The average O : C of CHON (Fig. S22b) and CHO (Fig. S22e) are both lower during the urban air masses period, suggesting that enhanced NO_x broadly suppresses autoxidation across organic compound classes.

Furthermore, as illustrated in Fig. S23, the mass concentration of SVOC ($-0.5 < \log_{10} C^* < 2.5 \mu\text{g m}^{-3}$) and LVOA ($-3.5 < \log_{10} C^* < -0.5 \mu\text{g m}^{-3}$, Donahue et al., 2012) in the gas phase exhibited an increase ($2.5 \mu\text{g m}^{-3}$ at $\text{NO}_x < 10 \text{ ppbv}$ vs. $3.3 \mu\text{g m}^{-3}$ at $\text{NO}_x \geq 30 \text{ ppbv}$) with the increase in NO_x , suggesting that these species likely contributed to the formation of Day- HNO_x -LVOA. Xu et al. (2014) found that both SOA volatility and oxidation state exhibited a non-linear response to NO_x in a series of chamber environment. SOA volatility decreases with increasing NO_x level when the ratio of initial NO to isoprene was lower than 3. At higher NO_x level, higher volatile SOA was produced, probably owing to the more competitive $\text{RO}_2 + \text{NO}$ pathway. Figure 5c1 and c2 investigate the relationship between these two factors and NO_3^-/SIA . Day- HNO_x -LVOA had a weak correlation ($R = 0.30$) with NO_3^-/SIA , while this trend overturned ($R = -0.35$) for Day- LNO_x -LVOA. Yang et al. (2022) showed that $\text{OH} + \text{NO}_2$ pathway mainly contribute to the formation of nitrate in this campaign. Together, these results indicate that elevated NO_x suppressed the formation of highly oxygenated organic compounds, thereby limiting the contribution to Day- LNO_x -LVOA. Thus, the Day- LNO_x -LVOA was more likely formed via gas-particle partitioning under relatively low NO_x condition.

It is worth noting that $\text{C}_4\text{H}_7\text{NO}_5$, likely originating from isoprene photooxidation in the presence of NO_x (Fisher et al., 2016; Paulot et al., 2009), also show a higher fraction in Day- LNO_x -LVOA (9.36×10^{-5} vs. 4.93×10^{-11} in Day- HNO_x -LVOA). A plausible explanation is that Heshan site, located at a suburban region, experienced ambient NO_x levels ($\sim 13 \text{ ppb}$ in the afternoon) sufficient to facilitate the formation of $\text{C}_4\text{H}_7\text{NO}_5$. It is further supported by the observation that both particle- and gas-phase $\text{C}_4\text{H}_7\text{NO}_5$ showed no significant variation with increasing NO_x (Fig. S24).

For the two urban-related factors, a positive correlation with O_x was observed only during the urban air masses period ($R = 0.46$ and 0.64 vs. -0.05 and 0.28 in the long-range transport period, Fig. S20a and c). Notably, Day-urban-LVOA increased from ~ 1.0 to $\sim 2.6 \mu\text{g m}^{-3}$ as O_x rose from 75 – $275 \mu\text{g m}^{-3}$ during this period, while it remained relatively stable ($\sim 0.4 \mu\text{g m}^{-3}$) during the long-range transport period (Fig. S25). In addition, Day-urban-LVOA showed only a limited similarity in its variation trend to Day- HNO_x -LVOA during the urban air mass period (Fig. S26). This finding supports the hypothesis that the daytime formation of urban-related OA factors was closely related to the urban

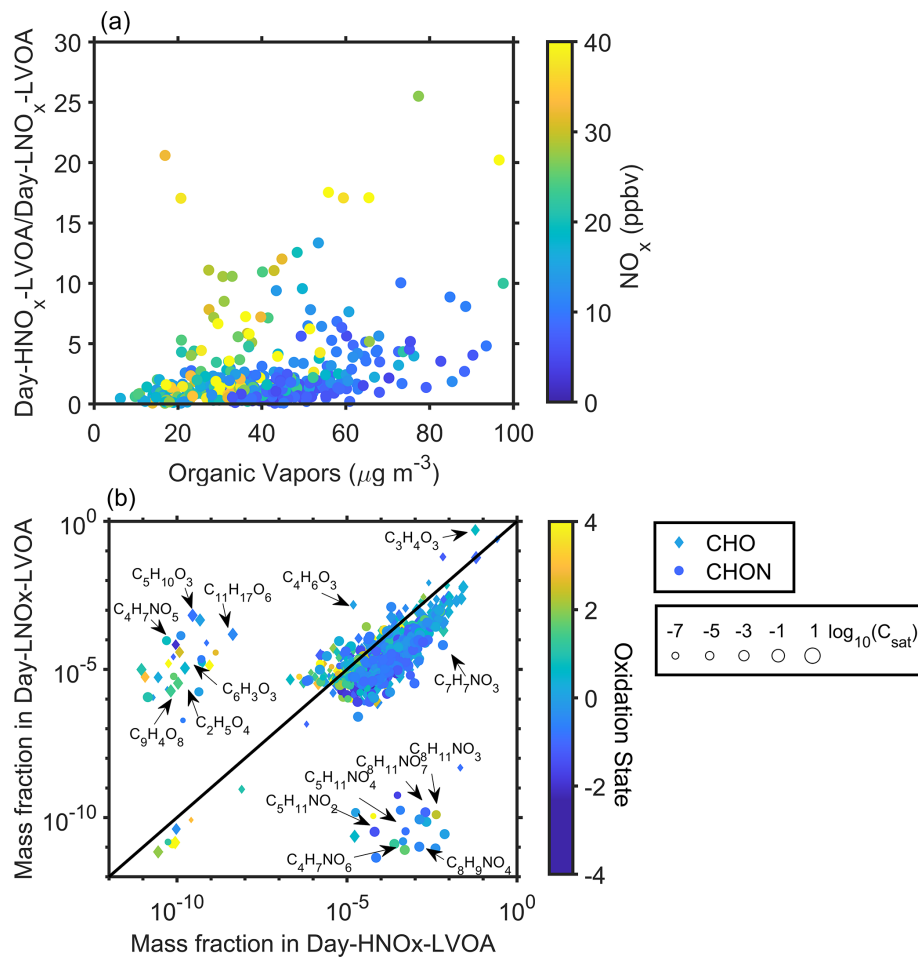


Figure 6. (a) Correlation between organic vapors and the ratio of Day-HNO_x-LVOA to Day-LNO_x-LVOA. (b) Scatterplots of mass fraction of different species in Day-HNO_x-LVOA and Day-LNO_x-LVOA. The color of dots in panel (a) denotes the corresponding NO_x. The shape, size, and color of markers in panel (b) represents the class of species, volatility, and $\overline{\text{OS}}_{\text{C}}$, respectively.

pollutants. Additionally, Day-urban-ELVOA exhibited a positive correlation with organic vapors ($R = 0.65$, Fig. S25b), while such a correlation was not observed for Day-urban-LVOA. It implies that Day-urban-ELVOA may primarily form through gas-particle partitioning during the urban air mass period.

Day-urban-LVOA was also positively correlated with NO₃⁻/SIA (Fig. 5c), consistent with the concurrent enhancement of nitrate and SOA during haze episodes (Ye et al., 2023; Zheng et al., 2021). During the urban air masses period, nitrate demonstrates a bimodal diurnal variation with peaks in both the morning and afternoon (Fig. S27), the latter peak likely attributed to OH + NO₂ pathway (Yang et al., 2022). Day-urban-LVOA had a significant correlation ($R = 0.97$) with succinic acid (C₄H₆O₄) in the particle phase (Fig. S28), which was previously reported to form via multiphase reaction during haze episode in megacity (Zhao et al., 2018; Zheng et al., 2021). As shown in Fig. S29, Day-urban-LVOA also increased with the ratio of the aerosol liq-

uid water content (ALWC) to PM₁, further indicating that aqueous processes in urban plumes played an important role in its enhancement.

For the aging factors, Day-aged-LVOA and Day-aged-ELVOA exhibited peak concentrations about 3 h later (at about 18:00 LT, Fig. 4) than other day factors (15:00 LT). It suggests that the two aged factors might originate from the photochemical aging processes of preexisting organic aerosols. To further explore the formation and aging process of these daytime factors, we estimated their daytime enhancement (Δ). For factors peaked at 15:00 LT, the Δ was estimated as the difference between the average mass concentration during 00:00–06:00 LT and 12:00–18:00 LT. For factors peaking at about 18:00 LT, Δ was regarded as the difference between the average mass concentration during 06:00–12:00 and 15:00–21:00 LT, since these factors remained at a relatively high-level during nighttime probably owing to lower boundary layer height. The Δ Day-aged-LVOA showed strong positive correlations with Δ Day-

HNO_x -LVOA ($R = 0.73$), Δ Day-urban-LVOA ($R = 0.77$), and Δ Day-LNO_x-LVOA ($R = 0.64$, Fig. 7a), suggesting that its formation might be closely associated with the aging processes of these three factors. Similarly, Δ Day-aged-ELVOA was positively correlated with both Δ Day-LNO_x-LVOA ($R = 0.61$), Δ Day-urban-LVOA ($R = 0.67$), and Δ Day-urban-ELVOA ($R = 0.73$, Fig. 7c). In contrast, we did not observe such correlations between Δ Day-aged-ELVOA and Δ Day-HNO_x-LVOA ($R = 0.49$, Fig. 7c). It implies that the formation of Day-aged-ELVOA was likely more influenced by the aging of urban-related factors and Day-LNO_x-LVOA.

3.3 Comparison with AMS OA

Adopting PMF analysis to thermogram datasets provides valuable insights into the formation and aging processes of SOA. However, the representativeness of FIGAERO-OA still requires evaluation. Figure 8 compares FIGAERO-OA with AMS-OA during two different periods. In general, FIGAERO-OA could not explain MO-OOA and HOA identified in AMS OA, given that all thermogram factors had a weak correlation ($R = -0.18 - 0.36$) between these two factors (Table S2). MO-OOA, which had the highest O:C (1.0) among all AMS factors (0.32–1.0) (Cai et al., 2024), was likely low volatile, meaning that much of this fraction might not have been vaporized during the heating process. Xu et al. (2019) investigate the volatility of different OA factors using the TD + AMS method and found that MO-OOA evaporated $\sim 52\%$ at $T = 175\text{ }^{\circ}\text{C}$. Another TD + AMS field study in the North China Plain suggested that the volatility of MO-OOA varied with RH levels, more MO-OOA evaporate at higher RH levels ($\text{RH} > 70$, Xu et al., 2021), suggesting that MO-OOA compounds formed at high RH condition could be higher volatile. During this campaign, the RH varied from 25%–92% which likely caused variability in MO-OOA volatility and thus in the fraction desorbed at 175 °C. This variability might explain the low correlation between MO-OOA in AMS and all FIGAERO-OA factors. HOA mainly consists of hydrocarbon-like organic compounds, which could not be detected by the FIGAERO-CIMS. The iodide source of the FIGAERO-CIMS is selective towards multi-functional organic compounds (Lee et al., 2014), making it less sensitive to detection hydrocarbon-like species. Ye et al. (2023) preformed factorization analysis of data obtained from the FIGAERO-CIMS and AMS and suggested that FIGAERO-derived OA factors could not account for all primary OA components resolved by AMS, including COA, NOA, and HOA. These findings highlight the need for further investigations into the chemical characteristics of primary OA to better understand their emission signatures and atmospheric evolution.

BBSOA in AMS-OA had a bimodal diurnal distribution with an afternoon peak ($\sim 14:00\text{ LT}$) and an evening peak

($\sim 17:00\text{ LT}$, Fig. S30). The enhancement was more pronounced in the afternoon (~ 1.6 to $\sim 3.6\text{ }\mu\text{g m}^{-3}$) compared to the evening (~ 2.9 to $\sim 4.0\text{ }\mu\text{g m}^{-3}$). Thus, we classify both BBSOA and LOOA as daytime SOA. Six thermogram daytime factors could explain the majority (82 % on average) of daytime SOA with the explained fraction increasing from 78 % during the long-range transport period to 85 % during the urban air masses period (Fig. 8a and b). In both periods, the summed thermogram daytime factors exhibited a diurnal variation like that of LOOA + BBSOA (Fig. 8c and d). Thermogram daytime OA was close to AMS daytime OA in the morning but fell below AMS OA afternoon. The discrepancy in the afternoon could be related to the decrease in OA volatility through strong photochemical reactions. Since the heating temperature of the FIGAERO-CIMS was set at 175 °C, compounds of very low volatility might not have been fully detected. This discrepancy narrowed during the urban air masses, likely owing to the strong SOA formation through gas-particle partitioning, which increased OA volatility (Cai et al., 2024). The gap persisted overnight, owing to suppressed vertical mixing under lower boundary layer conditions.

FIGAERO-OA explained about 13 % of BBOA in AMS OA during the campaign and this ratio remained relatively stable across different periods compared with daytime SOA (Fig. 8a and b). Because BBOA is closely tied to local biomass burning activities, air mass variations likely had only a minor influence on its chemical characteristics. BB-LVOA showed a diurnal pattern similar to both BBOA in AMS-OA and levoglucosan (Fig. 9a), with an evening peak around 18:30 LT, confirming their close association with biomass burning emissions. For nighttime chemistry related factor, both Night-OA (from AMS) and Night-LVOA (from thermograms) increase during the nighttime, while they did not share a similar diurnal pattern (Fig. 9b). Night-LVOA peaked at about 20:00 LT and decreased after 04:00 LT, while Night-OA peaked later, at about 06:00 LT, and declined in the morning. It suggested that Night-LVOA identified by FIGAERO-CIMS might not be able to fully capture the evolution of organic compounds involved in nighttime chemistry, which can explain 48 % of Night-OA in AMS-OA. Given that the majority of organic compounds formed through the nighttime chemistry were oxygenated and could be detected by FIGAERO CIMS (Wu et al., 2021), we speculated that the volatility of organic compounds decreased overnight, resulting that some low volatility organic aerosols would not be fully vaporized during the heating process. Xu et al. (2019) found that nighttime MO-OOA exhibited lower volatility compared with daytime MO-OOA, likely due to differences in precursors, formation mechanisms, and meteorological conditions.

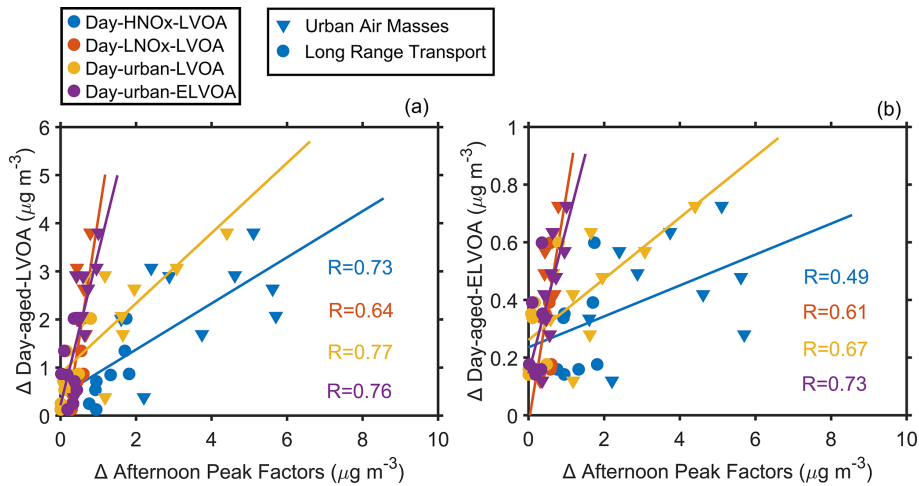


Figure 7. Correlation between the enhancement of (a) Day-aged-LVOA and afternoon peak factors and (b) Day-aged-ELVOA and afternoon peak factors. Afternoon peak factors include Day-HNO_x-LVOA, Day-LNO_x-LVOA, Day-urban-LVOA, and Day-urban-ELVOA. For afternoon peak factors, the enhancement (Δ) was regarded as the average mass concentration during 00:00–6:00 and 12:00–18:00 LT. For Day-aged-LVOA and Day-aged-ELVOA, the enhancement (Δ) was estimated as the difference between average mass concentration during 00:00–06:00 and 12:00–18:00 LT.

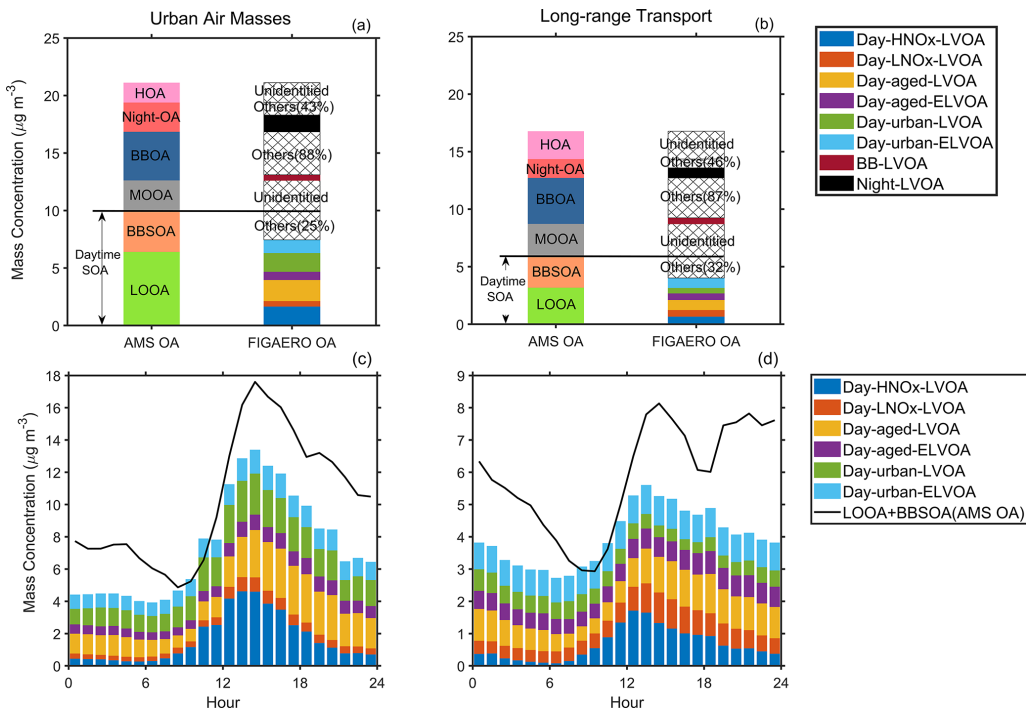


Figure 8. Comparison of the average mass concentration (a, b) and diurnal variation (c, d) of AMS-OA and FIGAERO-OA during long-range transport and urban air masses period.

4 Conclusions

In this study, we applied a PMF analysis to field thermogram data set measured by the FIGAERO-CIMS and classified the factors based on their potential formation pathways and volatility. Based on the PMF analysis to thermo-

grams data sets, six daytime OA factors, a biomass burning related factor, and nighttime chemistry related factor were identified. The formation of Day-HNO_x-LVOA and Day-LNO_x-LVOA was closely related to gas-particle partitioning, while Day-HNO_x-LVOA was observed to be formed with organic vapors under high NO_x condition. The increase in

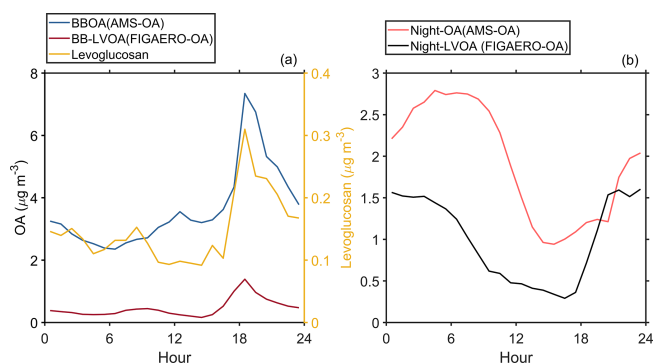


Figure 9. (a) Diurnal variation of BBOA from AMS, BB-LVOA and levoglucosan from FIGAERO-CIMS; (b) Diurnal variation of Night-OA from AMS, and Night-LVOA from FIGAERO-CIMS.

NO_x concentration might inhibit the production of highly oxygenated compounds (Cai et al., 2024), which could explain the relatively high volatility of Day- HNO_x -LVOA. Two urban related factors, Day-urban-LVOA and Day-urban-ELVOA, were identified, which only showed a daytime enhancement in urban plumes. The former might originate from aqueous processes, while the latter was likely formed through gas-particle partitioning. Our results demonstrated that photochemical-derived gas-particle partitioning mainly contributed to OA formation in downwind urban plumes.

Daytime aging processes of organic aerosol were observed and leading to the decrease in volatility with two aged factors (Day-aged-LVOA and Day-aged-ELVOA) identified. The formation of Day-aged-LVOA was related to the photochemical aging processes of Day- HNO_x -LVOA, Day- LNO_x -LVOA, Day-urban-LVOA, and Day-urban-ELVOA, while Day-aged-ELVOA originates from the aging processes of Day- LNO_x -LVOA, Day-urban-LVOA, and Day-urban-ELVOA. In general, these six thermogram daytime factors could explain the majority of daytime SOA in AMS OA, and this ratio increase from 79 % during the long-range transport period to 85 % during the urban air masses period, probably owing to a higher OA volatility (Cai et al., 2024). While FIGAERO-OA is unable to explain hydrocarbon like OA (HOA) and more oxygenated OA (MOOA), since the FIGAERO-CIMS could not detect hydrocarbon molecules and low volatility organic compounds with a volatilization temperature higher than 170 °C. For biomass-related OA, BB-LVOA could explain about 11 %–13 % of the BBOA in AMS OA, sharing a similar diurnal pattern, indicating that adopting a PMF analysis to thermogram profile could capture biomass burning events. While Night-LVOA had a different diurnal pattern with Night-OA in AMS OA, implying that this thermogram factor was not unable to represent the evolution of OA during the nighttime.

To our knowledge, existing field studies applying PMF to FIGAERO-CIMS data have primarily focused on the mass concentrations or signal intensities of organic compounds

rather than their thermograms. Chen et al. (2020) applied PMF to FIGAERO-CIMS datasets collected in Yorkville, GA, and reported substantial contributions of isoprene- and monoterpene-derived SOA during both daytime and nighttime. Using the same approach, Ye et al. (2023) showed that low- NO -like oxidation pathways played a significant role in SOA formation in urban environments. However, these PMF analyses did not provide volatility information, which limits our ability to fully understand the formation mechanisms and aging processes of OA. Lee et al. (2020) demonstrated that combining molecular-level composition measurements with volatility information enables the resolution of organic aerosol formation and aging pathways in the atmosphere, providing direct constraints on how oxidation processes alter both chemical functionality and volatility during aerosol evolution. Buchholz et al. (2020) performed PMF analysis on FIGAERO-CIMS thermogram datasets in laboratory experiments and demonstrated that both OA volatility and composition varied with relative humidity. Nevertheless, applications of thermogram-based PMF to ambient field measurements remain scarce.

Our results show that applying PMF directly to thermogram profiles from field observations yields additional and valuable volatility information that is not accessible from traditional mass- or signal-based PMF analyses. This added dimension is particularly useful for OA source apportionment. Along with PMF analysis of AMS or ACSM data, it can provide crucial information in understanding the formation and aging processes of OA. Using this method, we found that the daytime atmospheric evolution of SOA involved gas-particle partitioning, aqueous-phase reactions, and photochemical aging, highlighting the complexity of daytime SOA formation. Moreover, SOA volatility was strongly dependent on its formation pathways. Variations in NO_x not only influenced atmospheric oxidation but also modified SOA volatility by altering formation mechanisms. Nevertheless, further investigations are required to clarify the role of urban plumes in shaping SOA formation and its physicochemical properties.

Data availability. Data from the measurements are available at <https://doi.org/10.6084/m9.figshare.30155584> (Cai, 2025).

Supplement. The supplement related to this article is available online at <https://doi.org/10.5194/acp-26-769-2026-supplement>.

Author contributions. MC, WH, and BY designed the research. MC, BY, WH, YC, SH, SY, WC, YP, and JZ performed the measurements. MC, BY, WH, YC, SH, ZD, and DC analyzed the data. MC, WH and BY wrote the paper with contributions from all co-authors.

Competing interests. The contact author has declared that none of the authors has any competing interests.

Disclaimer. Publisher's note: Copernicus Publications remains neutral with regard to jurisdictional claims made in the text, published maps, institutional affiliations, or any other geographical representation in this paper. The authors bear the ultimate responsibility for providing appropriate place names. Views expressed in the text are those of the authors and do not necessarily reflect the views of the publisher.

Acknowledgements. Additional support from the crew of the Heshan supersite and Guangdong Environmental Monitoring Center is greatly acknowledged.

Financial support. This work was supported by Guangdong Basic and Applied Basic Research Foundation (grant nos. 2024A1515030221, 2023A1515012240), National Natural Science Foundation of China (grant nos. 42305123, 42375105), Science and Technology Projects in Guangzhou (grant no. 2025A04J4493), the Key Innovation Team of Guangdong Meteorological Bureau (GRMCTD202506-ZD06), and Central Public interest Scientific Institution Basal Research Fund of South China Institute of Environmental Sciences, MEE (grant no. PM-zx097-202506-214).

Review statement. This paper was edited by Mingyi Wang and reviewed by two anonymous referees.

References

Al-Naiema, I. M., Hettiyadura, A. P. S., Wallace, H. W., Sanchez, N. P., Madler, C. J., Cevik, B. K., Bui, A. A. T., Kettler, J., Griffin, R. J., and Stone, E. A.: Source apportionment of fine particulate matter in Houston, Texas: insights to secondary organic aerosols, *Atmos. Chem. Phys.*, 18, 15601–15622, <https://doi.org/10.5194/acp-18-15601-2018>, 2018.

Apte, J. S., Brauer, M., Cohen, A. J., Ezzati, M., and Pope III, C. A.: Ambient PM_{2.5} Reduces Global and Regional Life Expectancy, *Environ. Sci. Tech. Lett.*, 5, 546–551, <https://doi.org/10.1021/acs.estlett.8b00360>, 2018.

Arias, P. A., Bellouin, N., Coppola, E., Jones, R. G., Krinner, G., Marotzke, J., Naik, V., Palmer, M. D., Plattner, G. K., Rogelj, J., Rojas, M., Sillmann, J., Storelvmo, T., Thorne, P. W., Trewin, B., Achuta Rao, K., Adhikary, B., Allan, R. P., Armour, K., Bala, G., Barimalala, R., Berger, S., Canadell, J. G., Cassou, C., Cherchi, A., Collins, W., Collins, W. D., Connors, S. L., Corti, S., Cruz, F., Dentener, F. J., Dereczynski, C., Di Luca, A., Diongue Niang, A., Doblas-Reyes, F. J., Dosio, A., Douville, H., Engelbrecht, F., Eyring, V., Fischer, E., Forster, P., Fox-Kemper, B., Fuglestvedt, J. S., Fyfe, J. C., Gillett, N. P., Goldfarb, L., Gorodetskaya, I., Gutierrez, J. M., Hamdi, R., Hawkins, E., Hewitt, H. T., Hope, P., Islam, A. S., Jones, C., Kaufman, D. S., Kopp, R. E., Kosaka, Y., Kossin, J., Krakovska, S., Lee, J. Y., Li, J., Mauritsen, T., Maycock, T. K., Meinshausen, M., Min, S. K., Monteiro, P. M. S., Ngo-Duc, T., Otto, F., Pinto, I., Pirani, A., Raghavan, K., Ranasinghe, R., Ruane, A. C., Ruiz, L., Sallée, J. B., Samset, B. H., Sathyendranath, S., Seneviratne, S. I., Sörensson, A. A., Szopa, S., Takayabu, I., Tréguier, A. M., van den Hurk, B., Vautard, R., von Schuckmann, K., Zaehle, S., Zhang, X., and Zickfeld, K.: Technical Summary, in: *Climate Change 2021: The Physical Science Basis. Contribution of Working Group I to the Sixth Assessment Report of the Intergovernmental Panel on Climate Change*, edited by: Masson-Delmotte, V., Zhai, P., Pirani, A., Connors, S. L., Péan, C., Berger, S., Caud, N., Chen, Y., Goldfarb, L., Gomis, M. I., Huang, M., Leitzell, K., Lonnoy, E., Matthews, J. B. R., Maycock, T. K., Waterfield, T., Yelekçi, O., Yu, R., and Zhou, B., Cambridge University Press, Cambridge, United Kingdom and New York, NY, USA, 33–144, <https://doi.org/10.1017/9781009157896.002>, 2021.

Barsanti, K. C. and Pankow, J. F.: Thermodynamics of the formation of atmospheric organic particulate matter by accretion reactions – Part 1: aldehydes and ketones, *Atmos. Environ.*, 38, 4371–4382, <https://doi.org/10.1016/j.atmosenv.2004.03.035>, 2004.

Buchholz, A., Ylisirniö, A., Huang, W., Mohr, C., Canagaratna, M., Worsnop, D. R., Schobesberger, S., and Virtanen, A.: Deconvolution of FIGAERO–CIMS thermal desorption profiles using positive matrix factorisation to identify chemical and physical processes during particle evaporation, *Atmos. Chem. Phys.*, 20, 7693–7716, <https://doi.org/10.5194/acp-20-7693-2020>, 2020.

Cai, M.: New insight into the formation and aging processes of organic aerosols from positive matrix factorization analysis to ambient FIGAERO–CIMS thermograms, figshare [data set], <https://doi.org/10.6084/m9.figshare.30155584>, 2025.

Cai, M., Ye, C., Yuan, B., Huang, S., Zheng, E., Yang, S., Wang, Z., Lin, Y., Li, T., Hu, W., Chen, W., Song, Q., Li, W., Peng, Y., Liang, B., Sun, Q., Zhao, J., Chen, D., Sun, J., Yang, Z., and Shao, M.: Enhanced daytime secondary aerosol formation driven by gas–particle partitioning in downwind urban plumes, *Atmos. Chem. Phys.*, 24, 13065–13079, <https://doi.org/10.5194/acp-24-13065-2024>, 2024.

Cai, Y., Ye, C., Chen, W., Hu, W., Song, W., Peng, Y., Huang, S., Qi, J., Wang, S., Wang, C., Wu, C., Wang, Z., Wang, B., Huang, X., He, L., Gligorovski, S., Yuan, B., Shao, M., and Wang, X.: The important contribution of secondary formation and biomass burning to oxidized organic nitrogen (OON) in a polluted urban area: insights from in situ measurements of a chemical ionization mass spectrometer (CIMS), *Atmos. Chem. Phys.*, 23, 8855–8877, <https://doi.org/10.5194/acp-23-8855-2023>, 2023.

Chacon-Madrid, H. J. and Donahue, N. M.: Fragmentation vs. functionalization: chemical aging and organic aerosol formation, *Atmos. Chem. Phys.*, 11, 10553–10563, <https://doi.org/10.5194/acp-11-10553-2011>, 2011.

Charan, S. M., Huang, Y., and Seinfeld, J. H.: Computational Simulation of Secondary Organic Aerosol Formation in Laboratory Chambers, *Chem. Rev.*, 119, 11912–11944, <https://doi.org/10.1021/acs.chemrev.9b00358>, 2019.

Canonaco, F., Crippa, M., Slowik, J. G., Baltensperger, U., and Prévôt, A. S. H.: SoFi, an IGOR-based interface for the efficient use of the generalized multilinear engine (ME-2) for the source apportionment: ME-2 application to aerosol mass spectrometer data, *Atmos. Meas. Tech.*, 6, 3649–3661, <https://doi.org/10.5194/amt-6-3649-2013>, 2013.

Chen, G., Sosedova, Y., Canonaco, F., Fröhlich, R., Tobler, A., Vlachou, A., Daellenbach, K. R., Bozzetti, C., Hueglin, C., Graf, P., Baltensperger, U., Slowik, J. G., El Haddad, I., and Prévôt, A. S. H.: Time-dependent source apportionment of submicron organic aerosol for a rural site in an alpine valley using a rolling positive matrix factorisation (PMF) window, *Atmos. Chem. Phys.*, 21, 15081–15101, <https://doi.org/10.5194/acp-21-15081-2021>, 2021a.

Chen, W. T., Shao, M., Lu, S. H., Wang, M., Zeng, L. M., Yuan, B., and Liu, Y.: Understanding primary and secondary sources of ambient carbonyl compounds in Beijing using the PMF model, *Atmos. Chem. Phys.*, 14, 3047–3062, <https://doi.org/10.5194/acp-14-3047-2014>, 2014.

Chen, W., Hu, W., Tao, Z., Cai, Y., Cai, M., Zhu, M., Ye, Y., Zhou, H., Jiang, H., Li, J., Song, W., Zhou, J., Huang, S., Yuan, B., Shao, M., Feng, Q., Li, Y., Isaacman-VanWertz, G., Stark, H., Day, D. A., Campuzano-Jost, P., Jimenez, J. L., and Wang, X.: Quantitative Characterization of the Volatility Distribution of Organic Aerosols in a Polluted Urban Area: Intercomparison Between Thermodenuder and Molecular Measurements, *J. Geophys. Res.-Atmos.*, 129, e2023JD040284, <https://doi.org/10.1029/2023JD040284>, 2024.

Chen, Y., Takeuchi, M., Nah, T., Xu, L., Canagaratna, M. R., Stark, H., Baumann, K., Canonaco, F., Prévôt, A. S. H., Huey, L. G., Weber, R. J., and Ng, N. L.: Chemical characterization of secondary organic aerosol at a rural site in the southeastern US: insights from simultaneous high-resolution time-of-flight aerosol mass spectrometer (HR-ToF-AMS) and FIGAERO chemical ionization mass spectrometer (CIMS) measurements, *Atmos. Chem. Phys.*, 20, 8421–8440, <https://doi.org/10.5194/acp-20-8421-2020>, 2020.

Chen, Y., Guo, H., Nah, T., Tanner, D. J., Sullivan, A. P., Takeuchi, M., Gao, Z., Vasilakos, P., Russell, A. G., Baumann, K., Huey, L. G., Weber, R. J., and Ng, N. L.: Low-Molecular-Weight Carboxylic Acids in the Southeastern U. S.: Formation, Partitioning, and Implications for Organic Aerosol Aging, *Environ. Sci. Technol.*, 55, 6688–6699, <https://doi.org/10.1021/acs.est.1c01413>, 2021b.

Decker, Z. C. J., Zarzana, K. J., Coggon, M., Min, K.-E., Pollack, I., Ryerson, T. B., Peischl, J., Edwards, P., Dubé, W. P., Markovic, M. Z., Roberts, J. M., Veres, P. R., Graus, M., Warneke, C., de Gouw, J., Hatch, L. E., Barsanti, K. C., and Brown, S. S.: Nighttime Chemical Transformation in Biomass Burning Plumes: A Box Model Analysis Initialized with Aircraft Observations, *Environ. Sci. Technol.*, 53, 2529–2538, <https://doi.org/10.1021/acs.est.8b05359>, 2019.

Donahue, N. M., Robinson, A. L., Stanier, C. O., and Pandis, S. N.: Coupled Partitioning, Dilution, and Chemical Aging of Semivolatile Organics, *Environ. Sci. Technol.*, 40, 2635–2643, <https://doi.org/10.1021/es052297c>, 2006.

Donahue, N. M., Epstein, S. A., Pandis, S. N., and Robinson, A. L.: A two-dimensional volatility basis set: 1. organic-aerosol mixing thermodynamics, *Atmos. Chem. Phys.*, 11, 3303–3318, <https://doi.org/10.5194/acp-11-3303-2011>, 2011.

Donahue, N. M., Kroll, J. H., Pandis, S. N., and Robinson, A. L.: A two-dimensional volatility basis set – Part 2: Diagnostics of organic-aerosol evolution, *Atmos. Chem. Phys.*, 12, 615–634, <https://doi.org/10.5194/acp-12-615-2012>, 2012.

Faxon, C., Hammes, J., Le Breton, M., Pathak, R. K., and Halkin, M.: Characterization of organic nitrate constituents of secondary organic aerosol (SOA) from nitrate-radical-initiated oxidation of limonene using high-resolution chemical ionization mass spectrometry, *Atmos. Chem. Phys.*, 18, 5467–5481, <https://doi.org/10.5194/acp-18-5467-2018>, 2018.

Feng, T., Wang, Y., Hu, W., Zhu, M., Song, W., Chen, W., Sang, Y., Fang, Z., Deng, W., Fang, H., Yu, X., Wu, C., Yuan, B., Huang, S., Shao, M., Huang, X., He, L., Lee, Y. R., Huey, L. G., Canonaco, F., Prevot, A. S. H., and Wang, X.: Impact of aging on the sources, volatility, and viscosity of organic aerosols in Chinese outflows, *Atmos. Chem. Phys.*, 23, 611–636, <https://doi.org/10.5194/acp-23-611-2023>, 2023.

Fisher, J. A., Jacob, D. J., Travis, K. R., Kim, P. S., Marais, E. A., Chan Miller, C., Yu, K., Zhu, L., Yantosca, R. M., Sulprizio, M. P., Mao, J., Wennberg, P. O., Crounse, J. D., Teng, A. P., Nguyen, T. B., St. Clair, J. M., Cohen, R. C., Romer, P., Nault, B. A., Wooldridge, P. J., Jimenez, J. L., Campuzano-Jost, P., Day, D. A., Hu, W., Shepson, P. B., Xiong, F., Blake, D. R., Goldstein, A. H., Misztal, P. K., Hanisco, T. F., Wolfe, G. M., Ryerson, T. B., Wisthaler, A., and Mikoviny, T.: Organic nitrate chemistry and its implications for nitrogen budgets in an isoprene- and monoterpenenrich atmosphere: constraints from aircraft (SEAC⁴RS) and ground-based (SOAS) observations in the Southeast US, *Atmos. Chem. Phys.*, 16, 5969–5991, <https://doi.org/10.5194/acp-16-5969-2016>, 2016.

Gaston, C. J., Lopez-Hilfiker, F. D., Whybrow, L. E., Hadley, O., McNair, F., Gao, H., Jaffe, D. A., and Thornton, J. A.: Online molecular characterization of fine particulate matter in Port Angeles, WA: Evidence for a major impact from residential wood smoke, *Atmos. Environ.*, 138, 99–107, <https://doi.org/10.1016/j.atmosenv.2016.05.013>, 2016.

Graham, E. L., Wu, C., Bell, D. M., Bertrand, A., Haslett, S. L., Baltensperger, U., El Haddad, I., Krejci, R., Riipinen, I., and Mohr, C.: Volatility of aerosol particles from NO₃ oxidation of various biogenic organic precursors, *Atmos. Chem. Phys.*, 23, 7347–7362, <https://doi.org/10.5194/acp-23-7347-2023>, 2023.

Guo, J., Zhou, S., Cai, M., Zhao, J., Song, W., Zhao, W., Hu, W., Sun, Y., He, Y., Yang, C., Xu, X., Zhang, Z., Cheng, P., Fan, Q., Hang, J., Fan, S., Wang, X., and Wang, X.: Characterization of submicron particles by time-of-flight aerosol chemical speciation monitor (ToF-ACSM) during wintertime: aerosol composition, sources, and chemical processes in Guangzhou, China, *Atmos. Chem. Phys.*, 20, 7595–7615, <https://doi.org/10.5194/acp-20-7595-2020>, 2020.

Hildebrandt Ruiz, L., Paciga, A. L., Cerully, K. M., Nenes, A., Donahue, N. M., and Pandis, S. N.: Formation and aging of secondary organic aerosol from toluene: changes in chemical composition, volatility, and hygroscopicity, *Atmos. Chem. Phys.*, 15, 8301–8313, <https://doi.org/10.5194/acp-15-8301-2015>, 2015.

Huang, R.-J., Zhang, Y., Bozzetti, C., Ho, K.-F., Cao, J.-J., Han, Y., Daellenbach, K. R., Slowik, J. G., Platt, S. M., Canonaco, F., Zotter, P., Wolf, R., Pieber, S. M., Bruns, E. A., Crippa, M., Ciarelli, G., Piazzalunga, A., Schwikowski, M., Abbaszade, G., Schnelle-Kreis, J., Zimmermann, R., An, Z., Szidat, S., Baltensperger, U., Haddad, I. E., and Prevot, A. S. H.: High secondary aerosol contribution to particulate pollution during haze events in China, *Na-*

ture, 514, 218–222, <https://doi.org/10.1038/nature13774>, <http://www.nature.com/nature/journal/vaop/ncurrent/abs/nature13774.html#supplementary-information>, 2014.

Huang, S., Wu, Z., Poulain, L., van Pinxteren, M., Merkel, M., Assmann, D., Herrmann, H., and Wiedensohler, A.: Source apportionment of the organic aerosol over the Atlantic Ocean from 53° N to 53° S: significant contributions from marine emissions and long-range transport, *Atmos. Chem. Phys.*, 18, 18043–18062, <https://doi.org/10.5194/acp-18-18043-2018>, 2018.

Huang, W., Saathoff, H., Shen, X., Ramisetty, R., Leisner, T., and Mohr, C.: Seasonal characteristics of organic aerosol chemical composition and volatility in Stuttgart, Germany, *Atmos. Chem. Phys.*, 19, 11687–11700, <https://doi.org/10.5194/acp-19-11687-2019>, 2019.

Huang, X.-F., He, L.-Y., Hu, M., Canagaratna, M. R., Sun, Y., Zhang, Q., Zhu, T., Xue, L., Zeng, L.-W., Liu, X.-G., Zhang, Y.-H., Jayne, J. T., Ng, N. L., and Worsnop, D. R.: Highly time-resolved chemical characterization of atmospheric submicron particles during 2008 Beijing Olympic Games using an Aerodyne High-Resolution Aerosol Mass Spectrometer, *Atmos. Chem. Phys.*, 10, 8933–8945, <https://doi.org/10.5194/acp-10-8933-2010>, 2010.

Iyer, S., Lopez-Hilfiker, F., Lee, B. H., Thornton, J. A., and Kurtén, T.: Modeling the Detection of Organic and Inorganic Compounds Using Iodide-Based Chemical Ionization, *J. Phys. Chem.-USA*, 120, 576–587, <https://doi.org/10.1021/acs.jpca.5b09837>, 2016.

Jenkin, M. E.: Modelling the formation and composition of secondary organic aerosol from α - and β -pinene ozonolysis using MCM v3, *Atmos. Chem. Phys.*, 4, 1741–1757, <https://doi.org/10.5194/acp-4-1741-2004>, 2004.

Jimenez, J. L., Canagaratna, M., Donahue, N., Prevot, A., Zhang, Q., Kroll, J. H., DeCarlo, P. F., Allan, J. D., Coe, H., and Ng, N. J. S.: Evolution of organic aerosols in the atmosphere, *Science*, 326, 1525–1529, 2009.

Jorga, S. D., Florou, K., Kaltsoudis, C., Kodros, J. K., Vasilakopoulou, C., Cirtog, M., Fouqueau, A., Picquet-Varrault, B., Nenes, A., and Pandis, S. N.: Nighttime chemistry of biomass burning emissions in urban areas: A dual mobile chamber study, *Atmos. Chem. Phys.*, 21, 15337–15349, <https://doi.org/10.5194/acp-21-15337-2021>, 2021.

Krieger, U. K., Siegrist, F., Marcolli, C., Emanuelsson, E. U., Gobel, F. M., Bilde, M., Marsh, A., Reid, J. P., Huisman, A. J., Riipinen, I., Hyttinen, N., Myllys, N., Kurtén, T., Bannan, T., Percival, C. J., and Topping, D.: A reference data set for validating vapor pressure measurement techniques: homologous series of polyethylene glycols, *Atmos. Meas. Tech.*, 11, 49–63, <https://doi.org/10.5194/amt-11-49-2018>, 2018.

Kroll, J. H. and Seinfeld, J. H.: Chemistry of secondary organic aerosol: Formation and evolution of low-volatility organics in the atmosphere, *Atmos. Environ.*, 42, 3593–3624, <https://doi.org/10.1016/j.atmosenv.2008.01.003>, 2008.

Kuang, Y., Huang, S., Xue, B., Luo, B., Song, Q., Chen, W., Hu, W., Li, W., Zhao, P., Cai, M., Peng, Y., Qi, J., Li, T., Wang, S., Chen, D., Yue, D., Yuan, B., and Shao, M.: Contrasting effects of secondary organic aerosol formations on organic aerosol hygroscopicity, *Atmos. Chem. Phys.*, 21, 10375–10391, <https://doi.org/10.5194/acp-21-10375-2021>, 2021.

Lee, B. H., D'Ambro, E. L., Lopez-Hilfiker, F. D., Schobesberger, S., Mohr, C., Zawadowicz, M. A., Liu, J., Shilling, J. E., Hu, W., Palm, B. B., Jimenez, J. L., Hao, L., Virtanen, A., Zhang, H., Goldstein, A. H., Pye, H. O. T., and Thornton, J. A.: Resolving Ambient Organic Aerosol Formation and Aging Pathways with Simultaneous Molecular Composition and Volatility Observations, *ACS Earth and Space Chemistry*, 4, 391–402, <https://doi.org/10.1021/acsearthspacechem.9b00302>, 2020.

Lee, B. H., Lopez-Hilfiker, F. D., Mohr, C., Kurtén, T., Worsnop, D. R., and Thornton, J. A.: An Iodide-Adduct High-Resolution Time-of-Flight Chemical-Ionization Mass Spectrometer: Application to Atmospheric Inorganic and Organic Compounds, *Environ. Sci. Technol.*, 48, 6309–6317, <https://doi.org/10.1021/es500362a>, 2014.

Lee, B. P., Li, Y. J., Yu, J. Z., Louie, P. K., and Chan, C. K.: Characteristics of submicron particulate matter at the urban roadside in downtown Hong Kong – Overview of 4 months of continuous high-resolution aerosol mass spectrometer measurements, *J. Geophys. Res.-Atmos.*, 120, 7040–7058, 2015.

Lopez-Hilfiker, F. D., Mohr, C., Ehn, M., Rubach, F., Kleist, E., Wildt, J., Mentel, Th. F., Lutz, A., Hallquist, M., Worsnop, D., and Thornton, J. A.: A novel method for online analysis of gas and particle composition: description and evaluation of a Filter Inlet for Gases and AEROSols (FIGAERO), *Atmos. Meas. Tech.*, 7, 983–1001, <https://doi.org/10.5194/amt-7-983-2014>, 2014.

Lopez-Hilfiker, F. D., Iyer, S., Mohr, C., Lee, B. H., D'Ambro, E. L., Kurtén, T., and Thornton, J. A.: Constraining the sensitivity of iodide adduct chemical ionization mass spectrometry to multifunctional organic molecules using the collision limit and thermodynamic stability of iodide ion adducts, *Atmos. Meas. Tech.*, 9, 1505–1512, <https://doi.org/10.5194/amt-9-1505-2016>, 2016.

Louvaris, E. E., Florou, K., Karnezi, E., Papanastasiou, D. K., Gkatzelis, G. I., and Pandis, S. N.: Volatility of source apportioned wintertime organic aerosol in the city of Athens, *Atmos. Environ.*, 158, 138–147, <https://doi.org/10.1016/j.atmosenv.2017.03.042>, 2017.

Lu, Q., Murphy, B. N., Qin, M., Adams, P. J., Zhao, Y., Pye, H. O. T., Efthathiou, C., Allen, C., and Robinson, A. L.: Simulation of organic aerosol formation during the Cal-Nex study: updated mobile emissions and secondary organic aerosol parameterization for intermediate-volatility organic compounds, *Atmos. Chem. Phys.*, 20, 4313–4332, <https://doi.org/10.5194/acp-20-4313-2020>, 2020.

Matsui, H., Koike, M., Takegawa, N., Kondo, Y., Griffin, R. J., Miyazaki, Y., Yokouchi, Y., and Ohara, T.: Secondary organic aerosol formation in urban air: Temporal variations and possible contributions from unidentified hydrocarbons, *J. Geophys. Res.-Atmos.*, 114, <https://doi.org/10.1029/2008JD010164>, 2009.

Nie, W., Yan, C., Huang, D. D., Wang, Z., Liu, Y., Qiao, X., Guo, Y., Tian, L., Zheng, P., Xu, Z., Li, Y., Xu, Z., Qi, X., Sun, P., Wang, J., Zheng, F., Li, X., Yin, R., Dallenbach, K. R., Bianchi, F., Petäjä, T., Zhang, Y., Wang, M., Schervish, M., Wang, S., Qiao, L., Wang, Q., Zhou, M., Wang, H., Yu, C., Yao, D., Guo, H., Ye, P., Lee, S., Li, Y. J., Liu, Y., Chi, X., Kerminen, V.-M., Ehn, M., Donahue, N. M., Wang, T., Huang, C., Kulmala, M., Worsnop, D., Jiang, J., and Ding, A.: Secondary organic aerosol formed by condensing anthropogenic vapours over China's megacities, *Nat. Geosci.*, 15, 255–261, <https://doi.org/10.1038/s41561-022-00922-5>, 2022.

Nie, W., Yan, C., Yang, L., Roldin, P., Liu, Y., Vogel, A. L., Molteni, U., Stolzenburg, D., Finkenzeller, H., Amorim, A., Bianchi, F., Curtius, J., Dada, L., Draper, D. C., Duplissy, J., Hansel, A., He, X.-C., Hofbauer, V., Jokinen, T., Kim, C., Lehtipalo, K., Nichman, L., Mauldin, R. L., Makhmutov, V., Mentler, B., Mizelli-Ojdanic, A., Petäjä, T., Quéléver, L. L. J., Schallhart, S., Simon, M., Tauber, C., Tomé, A., Volkamer, R., Wagner, A. C., Wagner, R., Wang, M., Ye, P., Li, H., Huang, W., Qi, X., Lou, S., Liu, T., Chi, X., Dommen, J., Baltensperger, U., El Haddad, I., Kirkby, J., Worsnop, D., Kulmala, M., Donahue, N. M., Ehn, M., and Ding, A.: NO at low concentration can enhance the formation of highly oxygenated biogenic molecules in the atmosphere, *Nat. Commun.*, 14, 3347, <https://doi.org/10.1038/s41467-023-39066-4>, 2023.

Nihill, K. J., Ye, Q., Majluf, F., Krechmer, J. E., Canagaratna, M. R., and Kroll, J. H.: Influence of the NO/NO₂ Ratio on Oxidation Product Distributions under High-NO Conditions, *Environ. Sci. Technol.*, 55, 6594–6601, <https://doi.org/10.1021/acs.est.0c07621>, 2021.

Ou, H. J., Cai, M. F., Liang, B. L., Sun, Q. B., Zhou, S. Z., Xu, Y. S., Ren, L. H., and Zhao, J.: Characterization, Sources, and Chemical Processes of Submicron Aerosols at a Mountain Site in Central China, *J. Geophys. Res.-Atmos.*, 128, e2022JD038258, <https://doi.org/10.1029/2022JD038258>, 2023.

Paatero, P. and Tapper, U.: Positive matrix factorization: A non-negative factor model with optimal utilization of error estimates of data values, *Environmetrics*, 5, 111–126, <https://doi.org/10.1002/env.3170050203>, 1994.

Pankow, J. F. and Asher, W. E.: SIMPO L.1: a simple group contribution method for predicting vapor pressures and enthalpies of vaporization of multifunctional organic compounds, *Atmos. Chem. Phys.*, 8, 2773–2796, <https://doi.org/10.5194/acp-8-2773-2008>, 2008.

Paulot, F., Crounse, J. D., Kjaergaard, H. G., Kroll, J. H., Seinfeld, J. H., and Wennberg, P. O.: Isoprene photooxidation: new insights into the production of acids and organic nitrates, *Atmos. Chem. Phys.*, 9, 1479–1501, <https://doi.org/10.5194/acp-9-1479-2009>, 2009.

Praske, E., Otkjær, R. V., Crounse, J. D., Hethcox, J. C., Stoltz, B. M., Kjaergaard, H. G., and Wennberg, P. O.: Atmospheric autoxidation is increasingly important in urban and suburban North America, *P. Natl. Acad. Sci. USA*, 115, 64–69, <https://doi.org/10.1073/pnas.1715540115>, 2018.

Pye, H. O. T., D'Ambro, E. L., Lee, B. H., Schobesberger, S., Takeuchi, M., Zhao, Y., Lopez-Hilfiker, F., Liu, J., Shilling, J. E., Xing, J., Mathur, R., Middlebrook, A. M., Liao, J., Welti, A., Graus, M., Warneke, C., de Gouw, J. A., Holloway, J. S., Ryerson, T. B., Pollack, I. B., and Thornton, J. A.: Anthropogenic enhancements to production of highly oxygenated molecules from autoxidation, *P. Natl. Acad. Sci. USA*, 116, 6641–6646, <https://doi.org/10.1073/pnas.1810774116>, 2019.

Qin, Y. M., Tan, H. B., Li, Y. J., Schurman, M. I., Li, F., Canonaco, F., Prévôt, A. S. H., and Chan, C. K.: Impacts of traffic emissions on atmospheric particulate nitrate and organics at a downwind site on the periphery of Guangzhou, China, *Atmos. Chem. Phys.*, 17, 10245–10258, <https://doi.org/10.5194/acp-17-10245-2017>, 2017.

Ren, S., Yao, L., Wang, Y., Yang, G., Liu, Y., Li, Y., Lu, Y., Wang, L., and Wang, L.: Volatility parameterization of ambient organic aerosols at a rural site of the North China Plain, *Atmos. Chem. Phys.*, 22, 9283–9297, <https://doi.org/10.5194/acp-22-9283-2022>, 2022.

Rissanen, M. P.: NO₂ Suppression of Autoxidation–Inhibition of Gas-Phase Highly Oxidized Dimer Product Formation, *ACS Earth and Space Chemistry*, 2, 1211–1219, <https://doi.org/10.1021/acsearthspacechem.8b00123>, 2018.

Rudich, Y., Donahue, N. M., and Mentel, T. F.: Aging of Organic Aerosol: Bridging the Gap Between Laboratory and Field Studies, *Annu. Rev. Phys. Chem.*, 58, 321–352, <https://doi.org/10.1146/annurev.physchem.58.032806.104432>, 2007.

Shrivastava, M., Andreae, M. O., Artaxo, P., Barbosa, H. M. J., Berg, L. K., Brito, J., Ching, J., Easter, R. C., Fan, J., Fast, J. D., Feng, Z., Fuentes, J. D., Glasius, M., Goldstein, A. H., Alves, E. G., Gomes, H., Gu, D., Guenther, A., Jathar, S. H., Kim, S., Liu, Y., Lou, S., Martin, S. T., McNeill, V. F., Medeiros, A., de Sá, S. S., Shilling, J. E., Springston, S. R., Souza, R. A. F., Thornton, J. A., Isaacman-VanWertz, G., Yee, L. D., Ynoue, R., Zaveri, R. A., Zelenyuk, A., and Zhao, C.: Urban pollution greatly enhances formation of natural aerosols over the Amazon rainforest, *Nat. Commun.*, 10, 1046, <https://doi.org/10.1038/s41467-019-08909-4>, 2019.

Thornton, J. A., Mohr, C., Schobesberger, S., D'Ambro, E. L., Lee, B. H., and Lopez-Hilfiker, F. D.: Evaluating Organic Aerosol Sources and Evolution with a Combined Molecular Composition and Volatility Framework Using the Filter Inlet for Gases and Aerosols (FIGAERO), *Accounts Chem. Res.*, 53, 1415–1426, <https://doi.org/10.1021/acs.accounts.0c00259>, 2020.

Tian, S. L., Pan, Y. P., and Wang, Y. S.: Size-resolved source apportionment of particulate matter in urban Beijing during haze and non-haze episodes, *Atmos. Chem. Phys.*, 16, 1–19, <https://doi.org/10.5194/acp-16-1-2016>, 2016.

Ulbrich, I. M., Canagaratna, M. R., Zhang, Q., Worsnop, D. R., and Jimenez, J. L.: Interpretation of organic components from Positive Matrix Factorization of aerosol mass spectrometric data, *Atmos. Chem. Phys.*, 9, 2891–2918, <https://doi.org/10.5194/acp-9-2891-2009>, 2009.

Uchida, K., Ide, Y., and Takegawa, N.: Ionization efficiency of evolved gas molecules from aerosol particles in a thermal desorption aerosol mass spectrometer: Laboratory experiments, *Aerosol Sci. Tech.*, 53, 86–93, <https://doi.org/10.1080/02786826.2018.1544704>, 2019.

Walser, M. L., Park, J., Gomez, A. L., Russell, A. R., and Nizkorodov, S. A.: Photochemical Aging of Secondary Organic Aerosol Particles Generated from the Oxidation of d-Limonene, *J. Phys. Chem.-US A*, 111, 1907–1913, <https://doi.org/10.1021/jp066293L>, 2007.

Wang, Y., Clusius, P., Yan, C., Dällenbach, K., Yin, R., Wang, M., He, X.-C., Chu, B., Lu, Y., Dada, L., Kangasluoma, J., Rantala, P., Deng, C., Lin, Z., Wang, W., Yao, L., Fan, X., Du, W., Cai, J., Heikkinen, L., Tham, Y. J., Zha, Q., Ling, Z., Junninen, H., Petäjä, T., Ge, M., Wang, Y., He, H., Worsnop, D. R., Kerminen, V.-M., Bianchi, F., Wang, L., Jiang, J., Liu, Y., Boy, M., Ehn, M., Donahue, N. M., and Kulmala, M.: Molecular Composition of Oxygenated Organic Molecules and Their Contributions to Organic Aerosol in Beijing, *Environ. Sci. Technol.*, 56, 770–778, <https://doi.org/10.1021/acs.est.1c05191>, 2022.

Wu, C., Bell, D. M., Graham, E. L., Haslett, S., Riipinen, I., Baltensperger, U., Bertrand, A., Giannoukos, S., Schoonbaert, J., El Haddad, I., Prevot, A. S. H., Huang, W., and Mohr, C.: Photolytically induced changes in composition and volatility of biogenic secondary organic aerosol from nitrate radical oxidation during night-to-day transition, *Atmos. Chem. Phys.*, 21, 14907–14925, <https://doi.org/10.5194/acp-21-14907-2021>, 2021.

Xu, L., Kollman, M. S., Song, C., Shilling, J. E., and Ng, N. L.: Effects of NO_x on the Volatility of Secondary Organic Aerosol from Isoprene Photooxidation, *Environ. Sci. Technol.*, 48, 2253–2262, <https://doi.org/10.1021/es404842g>, 2014.

Xu, W., Chen, C., Qiu, Y., Li, Y., Zhang, Z., Karnezi, E., Pandis, S. N., Xie, C., Li, Z., Sun, J., Ma, N., Xu, W., Fu, P., Wang, Z., Zhu, J., Worsnop, D. R., Ng, N. L., and Sun, Y.: Organic aerosol volatility and viscosity in the North China Plain: contrast between summer and winter, *Atmos. Chem. Phys.*, 21, 5463–5476, <https://doi.org/10.5194/acp-21-5463-2021>, 2021.

Xu, W., Xie, C., Karnezi, E., Zhang, Q., Wang, J., Pandis, S. N., Ge, X., Zhang, J., An, J., Wang, Q., Zhao, J., Du, W., Qiu, Y., Zhou, W., He, Y., Li, Y., Li, J., Fu, P., Wang, Z., Worsnop, D. R., and Sun, Y.: Summertime aerosol volatility measurements in Beijing, China, *Atmos. Chem. Phys.*, 19, 10205–10216, <https://doi.org/10.5194/acp-19-10205-2019>, 2019.

Xu, X., Wang, G., Gao, Y., Zhang, S., Chen, L., Li, R., Li, Z., and Li, R.: Smog chamber study on the NO_x dependence of SOA from isoprene photo-oxidation: implication on RO_2 chemistry, *J. Environ. Sci.*, 161, 752–760, <https://doi.org/10.1016/j.jes.2025.05.024>, 2025.

Yang, S., Yuan, B., Peng, Y., Huang, S., Chen, W., Hu, W., Pei, C., Zhou, J., Parrish, D. D., Wang, W., He, X., Cheng, C., Li, X.-B., Yang, X., Song, Y., Wang, H., Qi, J., Wang, B., Wang, C., Wang, C., Wang, Z., Li, T., Zheng, E., Wang, S., Wu, C., Cai, M., Ye, C., Song, W., Cheng, P., Chen, D., Wang, X., Zhang, Z., Wang, X., Zheng, J., and Shao, M.: The formation and mitigation of nitrate pollution: comparison between urban and suburban environments, *Atmos. Chem. Phys.*, 22, 4539–4556, <https://doi.org/10.5194/acp-22-4539-2022>, 2022.

Ye, C., Yuan, B., Lin, Y., Wang, Z., Hu, W., Li, T., Chen, W., Wu, C., Wang, C., Huang, S., Qi, J., Wang, B., Wang, C., Song, W., Wang, X., Zheng, E., Krechmer, J. E., Ye, P., Zhang, Z., Wang, X., Worsnop, D. R., and Shao, M.: Chemical characterization of oxygenated organic compounds in the gas phase and particle phase using iodide CIMS with FIGAERO in urban air, *Atmos. Chem. Phys.*, 21, 8455–8478, <https://doi.org/10.5194/acp-21-8455-2021>, 2021.

Ye, C., Liu, Y., Yuan, B., Wang, Z., Lin, Y., Hu, W., Chen, W., Li, T., Song, W., Wang, X., Lv, D., Gu, D., and Shao, M.: Low-NO-like Oxidation Pathway Makes a Significant Contribution to Secondary Organic Aerosol in Polluted Urban Air, *Environ. Sci. Technol.*, 57, 13912–13924, <https://doi.org/10.1021/acs.est.3c01055>, 2023.

Ylisirniö, A., Barreira, L. M. F., Pullinen, I., Buchholz, A., Jayne, J., Krechmer, J. E., Worsnop, D. R., Virtanen, A., and Schobesberger, S.: On the calibration of FIGAERO-ToF-CIMS: importance and impact of calibrant delivery for the particle-phase calibration, *Atmos. Meas. Tech.*, 14, 355–367, <https://doi.org/10.5194/amt-14-355-2021>, 2021.

Ylisirniö, A., Hytinen, N., Li, Z., Alton, M., Nissinen, A., Pullinen, I., Miettinen, P., Yli-Juuti, T., and Schobesberger, S.: The saturation vapor pressures of higher-order polyethylene glycols and achieving a wide calibration range for volatility measurements by FIGAERO-CIMS, *Atmos. Meas. Tech.*, 18, 6449–6464, <https://doi.org/10.5194/amt-18-6449-2025>, 2025.

Zhang, Q., Jimenez, J. L., Canagaratna, M. R., Ulbrich, I. M., Ng, N. L., Worsnop, D. R., and Sun, Y.: Understanding atmospheric organic aerosols via factor analysis of aerosol mass spectrometry: a review, *Anal. Bioanal. Chem.*, 401, 3045–3067, <https://doi.org/10.1007/s00216-011-5355-y>, 2011.

Zhang, Y.-L., El-Haddad, I., Huang, R.-J., Ho, K.-F., Cao, J.-J., Han, Y., Zotter, P., Bozzetti, C., Daellenbach, K. R., Slowik, J. G., Salazar, G., Prévôt, A. S. H., and Szidat, S.: Large contribution of fossil fuel derived secondary organic carbon to water soluble organic aerosols in winter haze in China, *Atmos. Chem. Phys.*, 18, 4005–4017, <https://doi.org/10.5194/acp-18-4005-2018>, 2018.

Zhao, W., Kawamura, K., Yue, S., Wei, L., Ren, H., Yan, Y., Kang, M., Li, L., Ren, L., Lai, S., Li, J., Sun, Y., Wang, Z., and Fu, P.: Molecular distribution and compound-specific stable carbon isotopic composition of dicarboxylic acids, oxocarboxylic acids and α -dicarbonyls in $\text{PM}_{2.5}$ from Beijing, China, *Atmos. Chem. Phys.*, 18, 2749–2767, <https://doi.org/10.5194/acp-18-2749-2018>, 2018.

Zheng, Y., Chen, Q., Cheng, X., Mohr, C., Cai, J., Huang, W., Shrivastava, M., Ye, P., Fu, P., Shi, X., Ge, Y., Liao, K., Miao, R., Qiu, X., Koenig, T. K., and Chen, S.: Precursors and Pathways Leading to Enhanced Secondary Organic Aerosol Formation during Severe Haze Episodes, *Environ. Sci. Technol.*, 55, 15680–15693, <https://doi.org/10.1021/acs.est.1c04255>, 2021.

Zhou, W., Xu, W., Kim, H., Zhang, Q., Fu, P., Worsnop, D. R., and Sun, Y.: A review of aerosol chemistry in Asia: insights from aerosol mass spectrometer measurements, *Environ. Sci.-Proc. Imp.*, 22, 1616–1653, <https://doi.org/10.1039/D0EM00212G>, 2020.